ENVIRONMENTAL EPIGENETICS

Environmental Epigenetics, 2025, **11(1)**, 1–18

DOI: https://doi.org/10.1093/eep/dvaf007
Advance Access Publication 20 March 2025
Research Article

Silencing *TET1* expression alters the epigenomic landscape and amplifies transcriptomic responses to allergen in airway epithelial cells

Anthony P. Brown[1], Sreeja Parameswaran[2,3,4], Lucy Cai[1], Sweeney Elston[1], Chi Pham[1], Artem Barski[3,4,5], Matthew T. Weirauch[2,3,4,5,6,7], Hong Ji[1,8,*]

[1]California National Primate Research Center, University of California Davis, Davis, CA 95616, United States
[2]Center for Autoimmune Genomics and Etiology, Cincinnati Children's Hospital Medical Center, Cincinnati, OH 45229, United States
[3]Division of Allergy and Immunology, Cincinnati Children's Hospital Medical Center, Cincinnati, OH 45229, United States
[4]Division of Human Genetics, Cincinnati Children's Hospital Medical Center, Cincinnati, OH 45229, United States
[5]Department of Pediatrics, University of Cincinnati College of Medicine, Cincinnati, OH 45267, United States
[6]Division of Biomedical Informatics, Cincinnati Children's Hospital Medical Center, Cincinnati, OH 45229, United States
[7]Division of Developmental Biology, Cincinnati Children's Hospital Medical Center, Cincinnati, OH 45229, United States
[8]Department of Anatomy, Physiology and Cell biology, School of Veterinary Medicine, University of California Davis, Davis, CA 95616, United States

*Corresponding author. California National Primate Research Center, School of Veterinary Medicine, University of California Davis, Davis, CA 95616, United States. E-mail: hgji@ucdavis.edu

Abstract

Previous studies have demonstrated that ten-eleven translocation methylcytosine dioxygenase 1 (TET1) plays a protective role against house dust mite (HDM)-induced allergic airway inflammation. TET1 transcriptionally responded to HDM extract and regulated the expression of genes involved in asthma in human bronchial epithelial cells (HBECs). How TET1 regulates the expression of these genes, however, is unknown. To this end, we measured mRNA expression, DNA methylation, chromatin accessibility, and histone modifications in control and *TET1* knockdown HBECs treated or untreated with HDM extract. Throughout our analyses of multiomics data, we detected significant similarities between the effects of *TET1* knockdown alone and the effects of HDM treatment alone, all enriched for asthma-related genes and pathways. One especially striking pattern was that both *TET1* knockdown and HDM treatment generally led to decreased chromatin accessibility at many of the same genomic loci. Transcription factor enrichment analyses indicated that altered chromatin accessibility following the loss of TET1 may affect, or be affected by, CCCTC-binding factor and CCAAT-enhancer-binding protein binding. Analysis of H3K27ac levels and comparison with existing datasets suggested a potential impact of TET1 on enhancer activity. *TET1* loss also led to changes in DNA methylation, but these changes were generally in regions where accessibility was not changing. Lastly, more significant transcriptomic changes were observed in HBEC cells with *TET1* knockdown compared to control cells following HDM challenges. Collectively, our data suggest that TET1 regulates gene expression through distinct mechanisms across various genomic regions in airway epithelial cells, restricting transcriptomic responses to allergen and potentially protecting against the development of asthma.

Keywords: TET1; asthma; transcription factor; chromatin accessibility; methylation; RNA-seq; ATAC-seq; whole-genome bisulfite sequencing; functional genomics; gene regulation

Introduction

It is estimated that >300 million people worldwide suffer from asthma [1], a heterogeneous and complex disease that is treatable but not curable [2]. The total cost of asthma in the USA in 2013, including losses due to missed school and work, asthma-related deaths, and medical costs, was $81.9 billion [3]. Probably due in part to the heterogeneous nature of the disease, the exact causes for why some individuals develop asthma while others do not are largely unknown. Multiple previous studies have linked epigenetic modifications to asthma prevalence and severity [4–8]. In particular, our previous studies indicate that ten-eleven translocation methylcytosine dioxygenase 1 (TET1) is a key epigenetic modulator in asthma [4, 9]. TET1 is a member of the TET enzyme family, comprised of three demethylases (TET1, TET2,

Received 27 September 2024; Revised 18 February 2025; Accepted 19 March 2025

and TET3). These enzymes convert 5-methyl-cytosine (5mC) to 5-hydroxymethylcytosine (5hmC), then on to 5-formylcytosine (5fC) and 5-carboxylcytosine (5caC) [10]. 5fC and 5caC can subsequently be replaced by an unmethylated cytosine via a thymine DNA glycosylase-dependent base excision repair process [11]. Methylation of the *TET1* promoter in nasal cells has been associated with severe asthma in children [7]. Meanwhile, higher global levels of 5hmC were observed in different tissues from asthmatics [7, 12] and individuals with allergic rhinitis [13]. Exposure to house dust mites (HDM) led to a transient increase of *TET1* expression in human bronchial epithelial cells (HBECs) [14], although longer exposure and higher doses may lead to a significant decrease [7, 9]. Paradoxically, a study using *TET1* knockout mice and HDM exposure (a well-established model for allergic airway inflammation) indicated that TET1 activity protects against HDM-induced allergic airway inflammation through regulation of interferon signalling and the aryl hydrocarbon receptor (AhR) pathway [9]. *TET1* expression has also been shown to be sensitive to a variety of other stimuli [15], including ethanol exposure [16], repeated cocaine administration [17], ionizing radiation [18], and oxidative stress induced by heavy metals [19].

Prior studies on the association between TET1 and allergic disease and exposures focused primarily on how TET1 regulates DNA methylation. TET1, however, can also impact gene regulation and expression through other mechanisms, such as by interacting with histone modifiers and transcription factors (TFs) [15, 20, 21]. For example, TET1 interacts with hMOF, a histone acetyltransferase that can acetylate H4K16, a mark that generally promotes transcription [15, 22]. TET1 has also been shown to bind directly to transcriptional regulators such as EGR-1 [20], SIN3A [21], and ETV2 [23]. Although prior studies have separately identified TET1 as a key regulator in allergic airway inflammation and as a regulator of histone modifications, no studies have analysed the role of TET1 in regulating chromatin accessibility following respiratory challenges.

In this study, we assessed how mRNA expression, DNA methylation, and chromatin accessibility changed in HBECs that had *TET1* knocked down and/or were challenged with HDM. We integrated RNA-sequencing (RNA-seq), whole-genome bisulfite sequencing (WGBS), and ATAC-sequencing (ATAC-seq) data, and combined them with computational analyses of TF binding and histone modifications and ChIP-seq analysis of an enhancer-specific histone modification (H3K27ac) to more comprehensively understand the role that TET1 plays in regulating responses to allergic challenges. We found that *TET1* knockdown and HDM treatment both individually had similar effects on gene regulation (especially chromatin accessibility), while combining them caused nonadditive effects. Regions that underwent changes in TET1-mediated DNA methylation were generally different physical locations than regions with changes in chromatin accessibility, suggesting separate regulatory mechanisms. These observations provide novel insights into the role of TET1 in the regulation of the epigenetic landscape in airway epithelial cells and may explain contributions of TET1 to asthma.

Materials and methods

HBEC growth and TET1 knockdown

HBECs (a cell line obtained from Dr John Minna's lab at UT Southwestern Medical Center [24]) were grown in 1× Keratinocyte-Serum Free Medium (K-SFM) supplemented with Epidermal Growth Factor, pituitary extract, and pen-strep (complete media). A 12-well plate was seeded with cultured HBEC with near confluent numbers and incubated overnight for attachment. After 24 h, the complete media was replaced with 1× K-SFM with no serum supplements (minimal media) and incubated for an additional 8 h. *TET1* was knocked down by adding 30 pmol/ml siRNA (Thermo Fisher Scientific, assay ID: 147894, targeting mRNA sequence: GTTTGTACAAACCGTAAGAAATG) and incubated for 24 h in minimal media. Following nontargeting control siRNA or *TET1* siRNA incubation, saline or HDM (Greer) was added to HBEC at a concentration of 25 μg/ml (25 μg dry weight, containing 4.7 μg protein, 0.142 μg Derp1, 2.15 endotoxin unit, 0.20ng/μl RNA) and incubated for another 24 h before collection. To summarize, there were four different sample types in our study: (i) wild-type (WT) saline, (ii) WT HDM, (iii) *TET1* knockdown (KD) saline, and (iv) KD HDM.

ATAC-seq sample processing, library preparation, and data analysis

ATAC-seq libraries were prepared for a total of 12 samples (initial $n = 3$ for WT saline, $n = 3$ for WT HDM, $n = 3$ for KD saline, $n = 3$ for KD HDM). Samples were prepared according to the Omni-ATAC-seq protocol (modified from Corces *et al.* [25]). Briefly, 50 000 viable cells were lysed and nuclei were extracted. Nuclei were then treated with transposase at 37°C for 30 min (Nx#-tde1, tagment DNA enzyme, Illumina). DNA was extracted using Zymo DNA Clean and Concentrator-5 Kit and libraries were prepared. Preamplification with five cycles was performed and qPCR was used to determine additional PCR cycles. Libraries were then cleaned up and their quality was determined by bioanalyser. Indexed libraries were then mixed and sequenced at the DNA technologies core at UC Davis across two sequencing runs on a NovaSeq 6000. The number of single-end 100 bp reads per library from samples used in the final study ranged from 21 to 83 million. ATAC-seq data were processed using the ENCODE ATAC-seq pipeline (v 2.0.0) [26, 27] (https://github.com/ENCODE-DCC/atac-seq-pipeline/tree/v2.0.0). Briefly, reads were mapped to hg38 using BowTie2 [28] and peaks were called using MACS2 [29] (https://github.com/macs3-project/MACS/tree/v2.2.4). Based on sample clustering and other QC metrics (see Supplementary Table 1), two samples from each sample group were selected for further downstream analysis. Principal component analysis and unsupervised clustering were used to evaluate data quality. Differential peaks were identified using MANorm2 [30]. We identified differentially accessible peaks [false discovery rate (FDR) ≤ 0.05, fold-change ≥ 2] in three different comparisons: (i) KD saline vs. WT saline, (ii) WT HDM vs. WT saline, and (iii) KD HDM vs. WT HDM.

TF-binding analysis

A modified version of HOMER [31] utilizing a log base 2 likelihood scoring system was used to calculate motif enrichment statistics in the differentially accessible chromatin using a large library of human position weight matrix binding site models contained in build 2.0 of the CisBP database [32]. The RELI method was used to calculate the significance of intersection between the differentially accessible chromatin and publicly available ChIP seq data (~10 000 TFs) [33].

RNA-seq sample processing and RNA-seq data analysis

RNA-seq libraries were prepared for a total of 12 samples across four sample types ($n = 4$ for WT saline, $n = 4$ for KD saline, $n = 2$ for WT HDM, $n = 2$ for KD HDM). RNA (0.5 μg per sample, all with RNA quality ≥ 7) was submitted for poly-A RNA library preparation and sequencing at Novogene on a NovaSeq 6000 (Sacramento, CA).

Four of the samples (two WT saline samples and two KD saline samples) were sequenced in a separate batch, in which different sets of siRNAs targeting Tet1 (Thermo Fisher Scientific, assay ID: 147893 and Santa Cruz, sc-90457) were used [9]. Each sample had 21–30 million paired-end, 150 bp reads (Supplementary Table 1). Read quality was assessed using FastQC [34]. Reads were dynamically trimmed using Trim Galore [35] with the following settings: bases with less than a quality score of 20 were trimmed, 10 bases were trimmed from the 5′ end of both read 1 and read 2, the adapter stringency was set to 6, and reads smaller than 50 bases after trimming were discarded. The reads were aligned to the human transcriptome (hg38) using Bowtie2 [28]. Transcripts were subsequently quantified using RSEM [36]. The data were then converted into DESeq2 [37] format using tximport [38]. We used DESeq2 [37] for differential expression analyses and for hierarchical clustering and principal component analyses. As we observed some sequencing batch effects in an initial principal component analysis, batch was included as a covariate in the model provided to DESeq2. Genes with an absolute shrunken fold change of at least 1.2 and an FDR of $\leq$0.05 were considered significantly differentially expressed (DE).

Chromatin immunoprecipitation followed by sequencing and data analysis

$1–2 \times 10^6$ cells were fixed with 0.8% formaldehyde for 3 min at RT and quenched with a glycine solution. Cells were lysed with buffer L1 (50 nM Hepes pH 8.0, 140 nM NaCl, 1 mM EDTA, 10% glycerol, 0.5% Igepal CA-630, 0.25% Triton X-100, 1 mM Na butyrate) plus protease inhibitor for 10 min at 4°C. Nuclei pellets were incubated in buffer L2 (200 mM NaCl, 1 mM EDTA, 0.5 mM EGTA, 10 mM Tris-HCl pH8.0) with protease inhibitor and 1 mM Na butyrate. Isolated nuclei were then sonicated in 130 μl TE + 0.1% SDS. After sonication, sheared chromatin (0.5–1 μg, the average length was 200–250 bp) was incubated with the appropriate amount of antibody [H3K27ac (active motif, 5 μg per reaction)]. IPed DNA was purified using Qiagen MiniElute Reaction clean-up kit, and libraries were made by the UC Davis DNA technologies core using standard TruSeq ChIP Library Preparation Kit (Illumina). We obtained 31–42 million 150 bp paired-end reads per sample (Supplementary Table 1) from the NovaSeq 6000 at the DNA Technologies and Expression Analysis Cores of the UC Davis Genome Center. H3K27ac ChIP-Seq was performed for a total of eight samples (two each from these sample groups: WT saline, KD saline, WT HDM, and KD HDM). We used SciDAP [39] to trim reads (via Trim Galore [35]), align data to the hg38 human reference genome (via Bowtie2 [28]), call peaks (via MACS2 [29]), identify differential H3K27ac presence between sample groups (via DiffBind [40]), and identify super-enhancers within each sample (via ROSE [41, 42]). For the super-enhancer identification, we used a stitching distance of 20 kb and a Transcription Start Site exclusion zone of 2.5 kb. After identifying super-enhancers within each sample, we found consensus super-enhancers for each sample group using BEDtools [43]. We first kept only super-enhancers that overlapped with at least one super-enhancer in the other sample from the same group (using BEDtools intersect), and then we merged those overlapping super-enhancers together (using BEDtools merge) to form consensus super-enhancers for each sample group. For between-sample group comparisons, we used BEDtools intersect to identify super-enhancers that were unique to one sample group vs. another sample group (e.g. KD saline vs. WT saline).

WGBS library preparation and data analysis

WGBS libraries were prepared for a total of eight samples (two each from these sample groups: WT saline, KD saline, WT HDM, and KD HDM) using Swift's Accel-NGS Methyl-Seq Kit. We checked the quality of the libraries using an Agilent 2100 Bioanalyzer, and we measured library concentration using a Qubit high-sensitivity DNA assay. Individually barcoded libraries were pooled for sequencing. The pool was then sequenced on one lane of a NovaSeq 6000 S4 flow cell at PE150 at the DNA Technologies and Expression Analysis Cores of the UC Davis Genome Center. After sequencing, reads were demultiplexed using the bcl2fastq Illumina software. The number of paired-end reads per sample ranged from 70 to 155 million (Supplementary Table 1).

We used the CpG_Me pipeline [35, 44–46] to process and align the WGBS data. Because of methylation biases at the 5′ and 3′ ends of reads, we trimmed 10 bases from the 3′ end of both reads, and 10 and 20 bases from the 5′ end of read 1 and read 2, respectively, using Trim Galore [35]. Bismark [45] was then used to align the trimmed reads to the hg38 human reference genome and to generate CpG count matrices, which were used in downstream analyses. MultiQC [46] was used for quality control of the fastq data and the alignments to the reference genome. Following the above data processing, differentially methylated regions (DMRs) were identified for three different comparisons: (i) KD saline vs. WT saline, (ii) WT HDM vs. WT saline, and (iii) KD HDM vs. WT HDM. We used DMRichR [47–49] to perform these differential methylation analyses. For our differential methylation analyses, we required at least 1× coverage for a CpG for all samples included in a given comparison ('coverage'), a minimum of 5 CpGs for a DMR ('minCpGs'), 10 permutations for large-scale methylation block detection ('maxBlockPerms') and for determining the significance of DMRs ('maxPerms'), and the single CpG coefficient required to discover testable background regions to be at least 0.05 ('cut-off'). For a region to be considered a DMR, we required an empirical *P*-value of $\leq$.01 and a methylation difference of at least 10%.

Genomic region annotation, gene ontology, pathway analysis, and significance of overlapping regions

Annotation of genomic regions for WGBS, ATAC-seq, and ChIP-seq analyses was done using a 'nearest-gene' approach via DMRichR [47–49]. All pathway analyses were performed using Ingenuity Pathway Analysis (IPA) (QIAGEN Inc., https://www.qiagenbioinformatics.com/products/ingenuitypathway-analysis). A cut-off of FDR $\leq$ 0.05 was applied for significance. Gene set enrichment analysis (GSEA) [50] was used to test gene-level associations between changes in gene expression and changes in either methylation or chromatin accessibility. To test whether region-based overlaps were greater than expected by chance, we performed Fisher's exact tests using BEDtools [43] (a cut-off of $P \leq .05$ was used to determine significance). We overlapped our significant regions with several datasets from other studies retrieved from the NCBI Gene Expression Omnibus: A549 CCCTC-binding factor (CTCF) binding sites (GSM1003606), A549 CCAAT-enhancer-binding protein (CEBP) binding sites (GSM935630), A549 topologically associating domains (TADs; GSE92819), and A549 H3K27ac sites (GSE118840). Candidate *cis*-regulatory elements (cCREs) from A549 were downloaded from https://screen.encodeproject.org/. H3K27ac asthma-associated peaks [51], significant asthma EWAS results [52, 53], differentially methylated positions and regions associated with

asthma severity [54], and differentially methylated positions associated with allergic sensitization and allergic asthma [55] were also compared to significant regions from our current study. We used the WashU epigenome browser [56] to simultaneously visualize ATAC-seq and WGBS data. For visualization purposes only, ATAC-seq data were normalized between samples based on average transcription start site enrichment.

IL1B enhancer reporter assay

HBECs were grown to 70% confluency in a 96-well plate using keratinocyte serum-free medium supplemented with human recombinant epidermal growth factor, Bovine Pituitary Extract (Life Technologies, Carlsbad, CA), and 1% Penicillin–Streptomycin (pen/strep) antibiotic (Thermo Fisher Scientific, Florence, KY). After 24 h, starving media (keratinocyte serum-free media+1% pen/strep) was administered. Control plasmid and IL1B enhancer plasmid (100 ng/well) were transfected using Lipofectamine 3000 (Thermo Fisher Scientific, Florence, KY), P3000 Reagent (Thermo Fisher Scientific, Florence, KY), and Opti-MEM medium (Thermo Fisher Scientific, Florence, KY) according to the manufacturer's protocol. After 24 h, the plate was read under fluorescence using a microplate reader (Molecular Devices VERSAmax) at the excitation wavelength of 482 and the emission wavelength of 502. The plasmid was custom-made by Vector Builder Inc., wherein the IL1B enhancer sequence was inserted into a plasmid that contains TurboGFP, a bright green fluorescent protein. For data analysis, the fluorescence readings for the empty wells were averaged and used as the average background. The average background was then subtracted from the fluorescence reading obtained from wells that had samples in them to normalize the data.

Results

Loss of *TET1* expression decreases chromatin accessibility in HBECs

In order to understand how TET1 regulates gene expression in HBECs, we attempted to knock down *TET1* expression using siRNAs and a CRISPR plasmid (Supplementary Fig. 1). We proceeded with one siRNA that significantly knocked down *TET1* (48-h incubation led to ~50% downregulation, Supplementary Fig. 1A) and examined the impact on chromatin accessibility using ATAC-seq. Compared to control WT saline cells, cells with deficient TET1 expression (KD saline) showed a general decrease in chromatin accessibility (Fig. 1, Table 1). Overall, we identified 6975 differentially accessible peaks (FDR ≤ 0.05, fold-change ≥ 2) in the KD saline vs. WT saline comparison, which were annotated to 4669 unique genes (Supplementary Table 2, selected candidates shown in Fig. 2 and Supplementary Fig. 2). These peaks were 408 bp on average and were primarily associated with introns (42.6%), distal intergenic regions (35.5%), promoters (9.4% within 3 kb of the transcription start site), or exons (8.4%). Compared to background regions, the peaks were enriched for 5′ Untranslated Regions (UTRs), exons, and intergenic regions, while depleted in promoters (Supplementary Fig. 3). The majority of these peaks (84.7%) were less accessible in KD saline cells. IPA analysis on the genes nearest to significantly differentially accessible ATAC-seq peaks revealed 111 significantly enriched canonical pathways (FDR ≤ 0.05; Supplementary Table 3, top pathways by cumulative absolute activation z-score shown in Fig. 3a). Some enriched pathways of interest included leukocyte extravasation signalling, IL-15 production, and pulmonary fibrosis idiopathic signalling pathway. Genes involved in oxidative stress response (e.g. *TLR3*, *TLR5*, *TLR10*, *ALDH1A1*, *ALDH1B1*, *ALDH2*, and *ALDH7A1*), type I immune response (e.g. *STAT3*, *STAT4*, *STAT5B*, *IFNGR1*, and *OAS1*), type II immune response (e.g. *STAT3*, *STAT4*, and *STAT5B*), and type 17 immune response (e.g. *AHR*, *AHRR*, and *IRF4*) all showed changes in accessibility (mostly reduced) when TET1 was low (Supplementary Table 2). Together, these data show that *TET1* expression promotes chromatin accessibility in HBECs.

Loss of *TET1* expression leads to changes in methylation, primarily in regions where chromatin accessibility did not change

It is well established that TET1 regulates DNA methylation [57] and that DNA methylation has a direct impact on TF binding [58, 59]. Some evidence suggests that DNA methylation may directly influence chromatin accessibility as well [60]. Therefore, we performed genome-wide bisulfite sequencing to evaluate the DNA methylation landscape in *TET1*-deficient HBECs. Given that TET1 is a demethylase, we expected that *TET1* knockdown samples would have generally higher methylation levels than samples where *TET1* was intact. However, this was not the case. When comparing *TET1* KD saline samples to WT saline samples, we identified 4359 significant DMRs (empirical *P*-value ≤ .01, ≥10% difference) annotated to 3224 unique genes (Supplementary Table 4). The DMRs were 898 bp on average, and most of the DMRs (~90%) were associated with introns (44%), intergenic regions (36%), or promoters (10%). Compared to background regions, these DMRs were enriched for promoters (Supplementary Fig. 3). Of these DMRs following *TET1* knockdown, 49.1% were hypermethylated (Fig. 1). These DMR-associated genes were enriched for 94 IPA pathways (FDR ≤ 0.05; Supplementary Table 5, top pathways in Fig. 3b). Enriched pathways of interest include pulmonary fibrosis idiopathic signalling pathway, IL-8 signalling, and IL-15 production. Out of these 4359 DMRs between KD saline and WT saline, only 14 had overlapping coordinates with one of the 5479 differentially accessible regions between these two sample groups (Fig. 4a). Collectively, although WGBS measures the sum of 5mC and 5hmC and may miss regions that undergo simultaneous and similar opposite changes in both marks [61], these data suggest that TET1 independently influences chromatin accessibility and DNA methylation in HBECs.

TET1 knockdown-induced chromatin accessibility and methylation changes influence gene expression

We next performed RNA-seq to assess the effect of *TET1* knockdown on gene expression and to attempt to correlate changes in gene expression with changes in chromatin accessibility and/or DNA methylation. We identified 5242 genes that were DE in the KD saline vs. WT saline comparison (Supplementary Table 6). There was a fairly even split of upregulation and downregulation in these DE genes (51.9% upregulated, Fig. 1). These DE genes were enriched for IPA pathways of interest such as IL-8 signalling, HIF1α signalling, AhR signalling, and NRF2-mediated oxidative stress response (Supplementary Table 7, top pathways in Fig. 3c). Importantly, some of these changes in gene expression correlated with changes in DNA methylation and chromatin accessibility following *TET1* knockdown. Genes near regions with changes in accessibility tended to have reduced expression in KD saline (Fig. 5a). Genes with more accessible promoters in KD saline showed a trend for increased expression (FDR = 0.123, Fig. 5b), while genes with less accessible promoters were significantly more likely to have decreased gene expression (FDR = 0.008, Fig. 5c). Genes near DMRs were significantly more likely to be downregulated in KD saline (FDR = ~0, Fig. 5d). Genes with hypermethylated promoters in KD saline showed a trend of having decreased expression

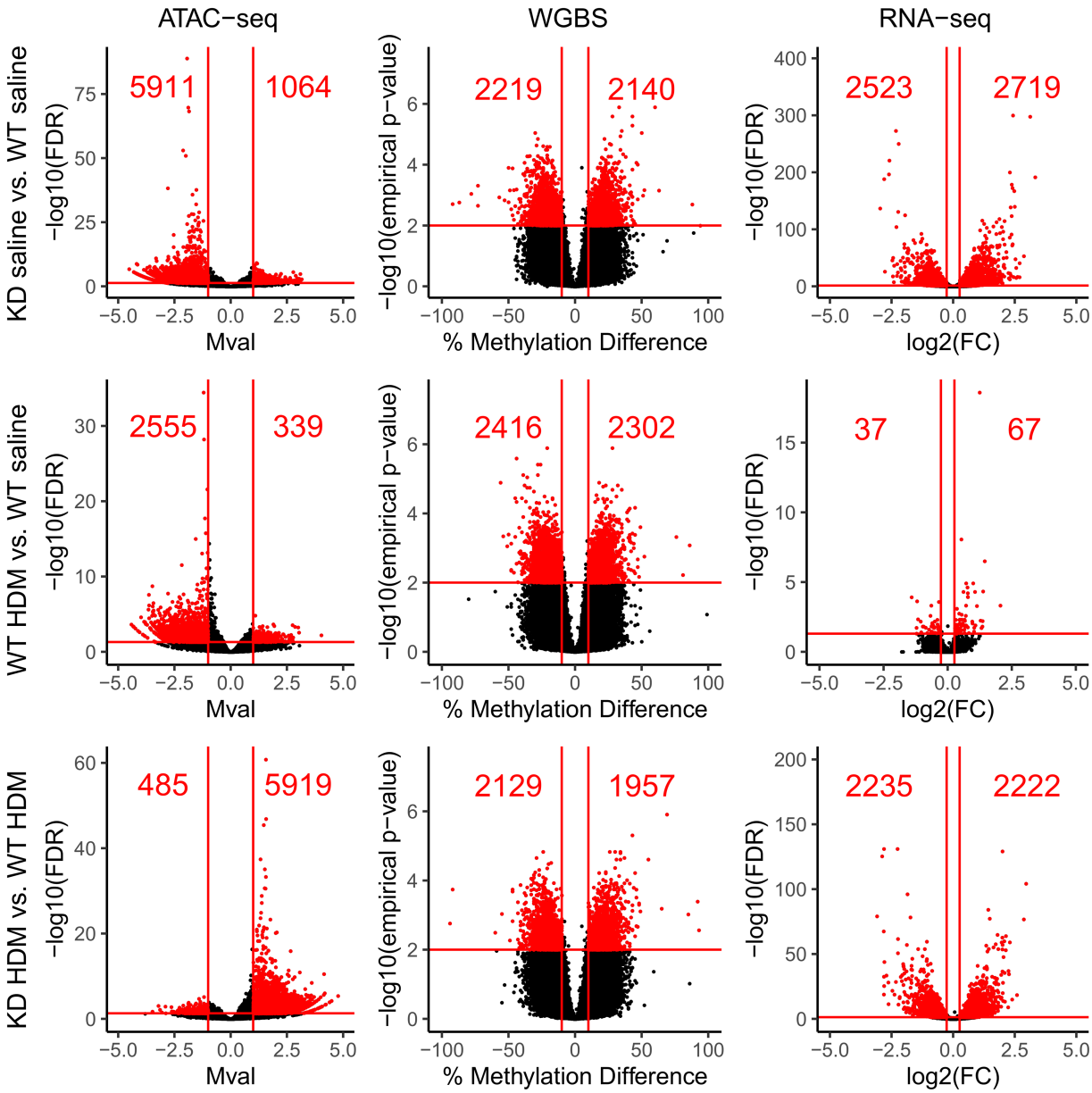

Figure 1. TET1- and HDM-specific chromatin accessibility, DNA methylation, and gene expression.

Volcano plots depicting condition-specific changes. Dots in the upper left and upper right quadrants show significant differences: for ATAC-seq, differentially accessible peaks required an FDR of ≤0.05 and a fold change of at least 2. For WGBS, DMRs required an empirical *P*-value of ≤0.01 with at least a 10% difference in methylation percentage. For RNA-seq, DE genes required an FDR of ≤0.05 and a fold change of at least 1.2. The numbers above the plots represent the number of significant results on that side of the plot (e.g. 2523 is the number of genes that had decreased expression in KD saline vs. WT saline). WT saline = *TET1* intact saline samples, WT HDM = *TET1* intact HDM samples, KD saline = *TET1* knockdown saline samples, KD HDM = *TET1* knockdown HDM samples, Mval = difference in mean signal intensity between the two conditions.

(FDR = 0.116, Fig. 5e), while genes with hypomethylated promoters showed a trend of having increased expression (FDR = 0.209, Fig. 5f). DE genes with increased accessibility at their promoters on average had increased expression in KD saline ($P = .06$, Supplementary Fig. 4A), while DE genes with any change in methylation (regardless of direction) at their promoters on average had increased expression in KD saline as well ($P = .21$, Supplementary Fig. 4B). Via Spearman's rank correlation coefficient, we noted a significant positive correlation in DE genes between changes in accessibility and expression (Fig. 5g, Spearman's $r_s = 0.18$, right-tailed $P = .03$), and a nonsignificant negative correlation in DE genes between changes in methylation and expression (Fig. 5h, Spearman's $r_s = -0.11$, left-tailed $P = .15$) in KD saline vs. WT saline. Genes showing strong correlation in accessibility and expression include *ALDH1A1*, *PBX1*, *ACSS1*, *PLXNC1*, and *HOPX* (Fig. 5g), while genes showing strong correlation in methylation and expression include *EMP2*, *APOL3*, and *LINC02541* (Fig. 5h). Overall, these analyses show a stronger correlation between changes in accessibility and expression than changes in methylation and expression in KD saline vs. WT saline.

To further compare the effects of methylation and accessibility on gene expression, we also performed IPA pathway analyses on genes that were both associated with a DMR and DE following *TET1* knockdown (but not differentially accessible, DMR + DE only). These genes (7.2% of all DE genes, Fig. 4b) were enriched for nine IPA canonical pathways (FDR ≤ 0.05; Supplementary Table 8).

Table 1. Results summary table broken down by analysis

Chromatin accessibility/ATAC-seq	• TET1 knockdown and HDM treatment each generally led to decreased chromatin accessibility • There was significant overlap in the effects of TET1 knockdown and HDM treatment on chromatin accessibility; all overlapping peaks showed changes in the same direction • Combining TET1 knockdown with HDM treatment generally led to increased chromatin accessibility • Loss of TET1 may affect, or be affected by, CTCF and CEBP binding • TET1 knockdown and HDM treatment (separately and combined) led to some regions increasing in methylation and some regions decreasing in methylation
Methylation/WGBS	• There was a significant overlap in changes induced by TET1 knockdown and HDM treatment, but there was less overlap in methylation changes than in accessibility changes • Methylation changes were not enriched for TF-binding sites
H3K27ac ChIP-seq	• TET1 knockdown and HDM treatment (separately and together) generally led to decreased H3K27ac signal • There was significant overlap between H3K27ac changes induced by TET1 knockdown and HDM treatment • H3K27ac changes suggest that TET1 knockdown and HDM treatment may affect the distribution of super-enhancers
Expression/RNA-seq	• TET1 knockdown led to more differential expression than HDM treatment alone; TET1 knockdown potentiated the effects of HDM treatment • There was significant overlap between gene expression changes induced by TET1 knockdown and HDM treatment • Expression changes correlated better with chromatin accessibility changes than with methylation changes or H3K27ac changes.

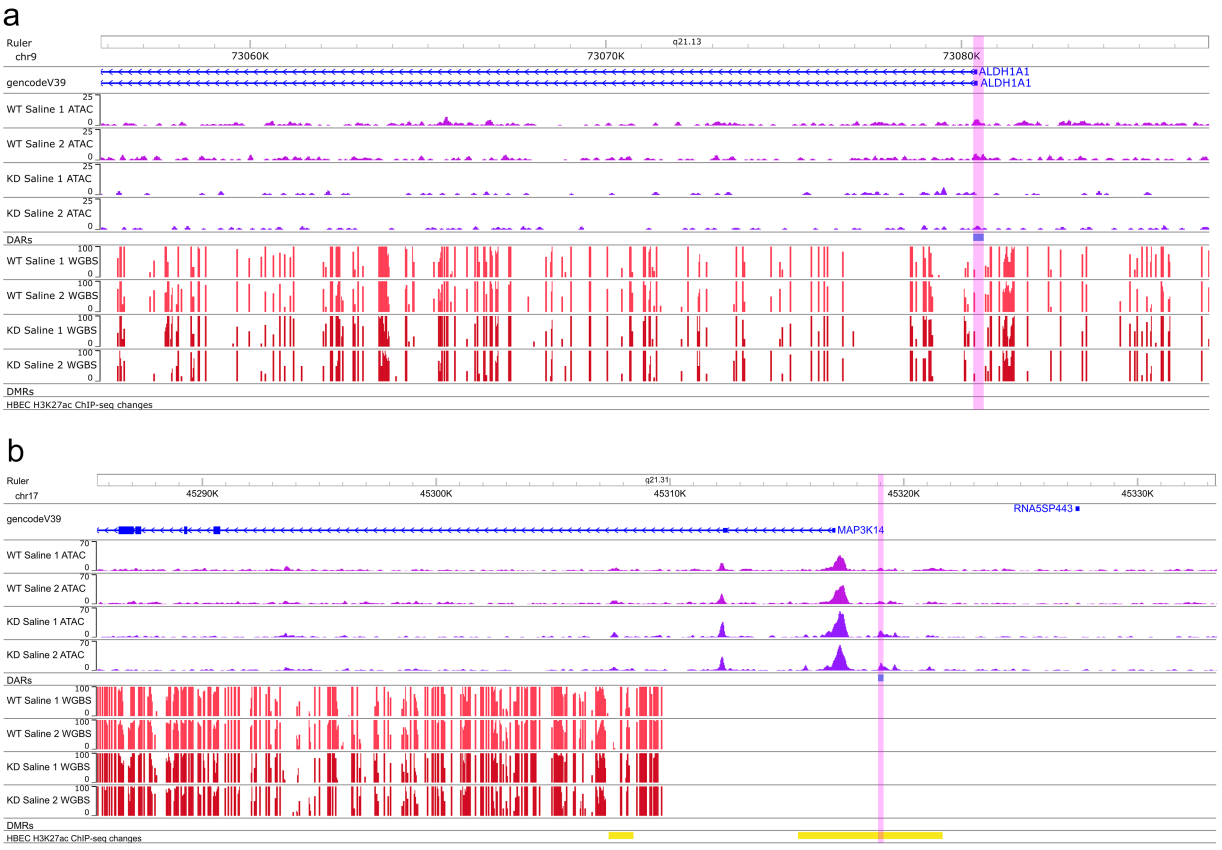

Figure 2. Changes in chromatin accessibility following *TET1* knockdown near genes of interest.

Changes in chromatin accessibility in (a) *ALDH1A1* (oxidative stress response) and (b) *MAP3K14* (Nfkb signalling) following *TET1* knockdown. The peak at *MAP3K14* overlaps with a region also showing differences in H3K27ac ChIP-seq levels. To approximate MANorm2-based data normalization, the ATAC data shown were normalized between samples based on average transcription start site enrichment (for visualization purposes only). The 'HBEC H3K27ac ChIP-seq changes' track is from data in our current study. Abbreviations: WT saline = *TET1* intact saline samples, KD saline = *TET1* knockdown saline samples, DARs = differentially accessible regions.

We compared these pathways to enriched pathways in genes that were simultaneously associated with a differentially accessible peak and DE, but not differentially methylated (ATAC + DE only). These genes (14.3% of all DE genes, Fig. 4b) were enriched for 132 IPA canonical pathways (Supplementary Table 8). Out of the nine enriched pathways from the DMR + DE-only set, seven were also enriched in the ATAC + DE-only set. On the other hand, some of the 126 pathways enriched in ATAC + DE only but not DMR + DE only include EIF2 signalling, IL-8 signalling, NRF2-mediated oxidative stress response, and xenobiotic metabolism signalling. There were also 228 genes (4.4% of all DE genes, Fig. 4b) that were simultaneously DE, differentially methylated, and differentially accessible

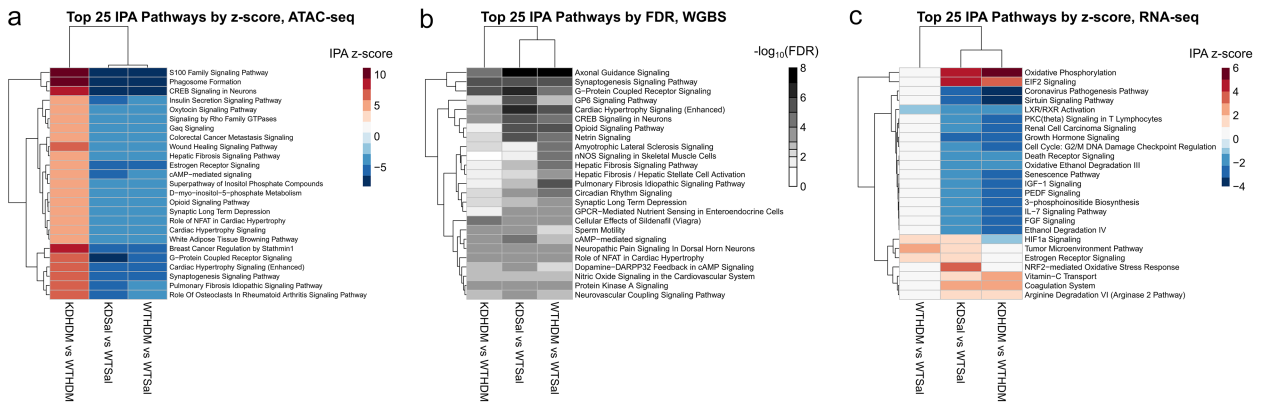

Figure 3. Pathway enrichment of differential ATAC-seq, WGBS, and RNA-seq following *TET1* knockdown and/or HDM treatment.

(a) Top 25 IPA canonical pathways by the total activation z-score from differentially accessible regions in each of the comparisons included in this study (KD saline vs. WT saline, WT HDM vs. WT saline, and KD HDM vs. WT HDM). Activation z-scores were calculated by assuming a positive correlation between chromatin accessibility and gene expression. A red colour indicates a positive z-score, indicating that IPA predicted that a given pathway would have increased activity. A blue colour indicates a negative z-score, indicating that IPA predicted that a given pathway would have decreased activity. (b) Top 25 IPA canonical pathways by the total FDR from DMRs in each of the comparisons included in this study. Given the context-dependent relationship between methylation and expression, activation z-scores could not reliably be calculated for the methylation data. (c) Top 25 IPA canonical pathways by the total activation z-score from DE genes in each of the comparisons included in this study. Abbreviations: WT saline = *TET1* intact saline samples, WT HDM = *TET1* intact HDM samples, KD saline = *TET1* knockdown saline samples, KD HDM = *TET1* knockdown HDM samples.

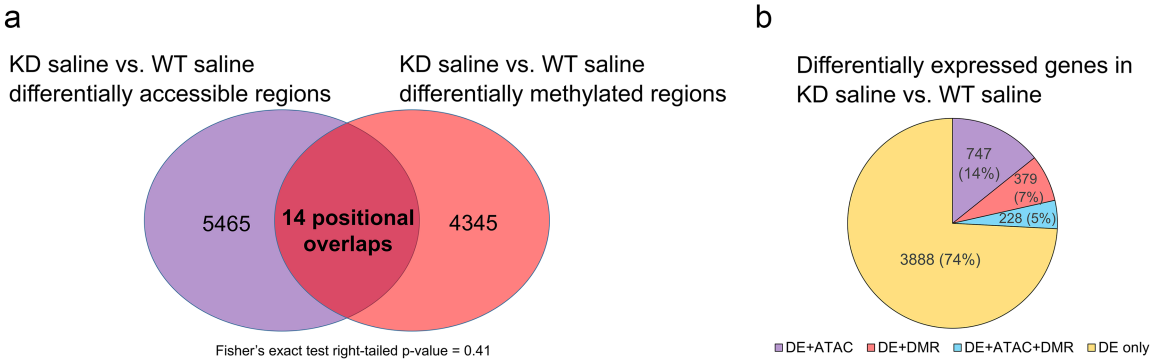

Figure 4. Changes in DNA methylation and chromatin accessibility affect different regions of the genome following *TET1* knockdown.

(a) Venn diagram showing positional overlaps between regions changing in accessibility and DNA methylation in KD saline vs. WT saline. There were no more overlaps than expected by chance ($P = .41$). (b) Pie chart showing overlaps at the gene level for differential expression (DE), differentially accessible regions (ATAC), and DMRs. Abbreviations: WT saline = *TET1* intact saline samples, KD saline = *TET1* knockdown saline samples, ATAC = differentially accessible regions.

(ATAC + DMR + DE). There was a physical overlap between the DMR and the differentially accessible region in only 14 of these genes. The ATAC + DMR + DE genes were only enriched for one IPA canonical pathway (protein kinase A signalling), and this pathway was not enriched in either the ATAC + DE-only group or the DMR + DE-only group. Overall, these results imply that changes in chromatin accessibility and DNA methylation following *TET1* knockdown both impact gene expression, but they often affect different genes, pathways, and regions of the genome.

HDM challenge closes chromatin in a similar fashion to *TET1* knockdown in HBECs

HDM promotes allergy and asthma in humans [62, 63]. We previously found that HDM challenge reduced the expression of Tet1 *in vivo*, and loss of TET1 exaggerated HDM-induced allergic airway inflammation in mice [9]. Our data also suggest that HDM challenge in HBECs may affect the expression of *TET1* [9]. In the RNA-seq experiments, HDM led to some trend of downregulation of TET1 expression after 24 h (Supplementary Fig. 1). Therefore, we hypothesized that TET1 loss and HDM treatment have a similar impact on chromatin accessibility. We observed 2894 ATAC-seq peaks that were significantly different between WT HDM and WT saline cells (FDR ≤ 0.05, fold-change ≥ 2; Fig. 1, Supplementary Table 2, annotated to 2328 genes). These peaks were on average 408 bp and were primarily associated with introns (44%), intergenic regions (36%), exons (8%), and promoters (8%). Similar to those changes induced by *TET1* knockdown, these peaks were enriched for exons and intergenic regions, while depleted in promoters (Supplementary Fig. 3). HDM treatment also primarily led to decreased chromatin accessibility (88.3%) in regions where accessibility was altered (Fig. 1, Supplementary Fig. 5A). Of these peaks, 65.8% overlapped with a significant peak from the KD saline vs. WT saline comparison, significantly more than expected by chance ($P = \sim 0$, Fig. 6a). Even more striking is that for each overlap, the direction of change in the HDM-treated group was the same as the direction of change in the KD saline group (i.e. if accessibility increased in KD saline vs. WT saline, it also increased in WT HDM vs. WT saline). A principal component analysis on the chromatin accessibility data revealed that WT HDM samples clustered closest with KD saline samples, with these two groups split from WT saline and KD HDM along PC1 (Supplementary Fig. 6). Genes associated with differentially accessible peaks were significantly enriched for 88 IPA pathways (FDR ≤ 0.05; Fig. 3a, Supplementary

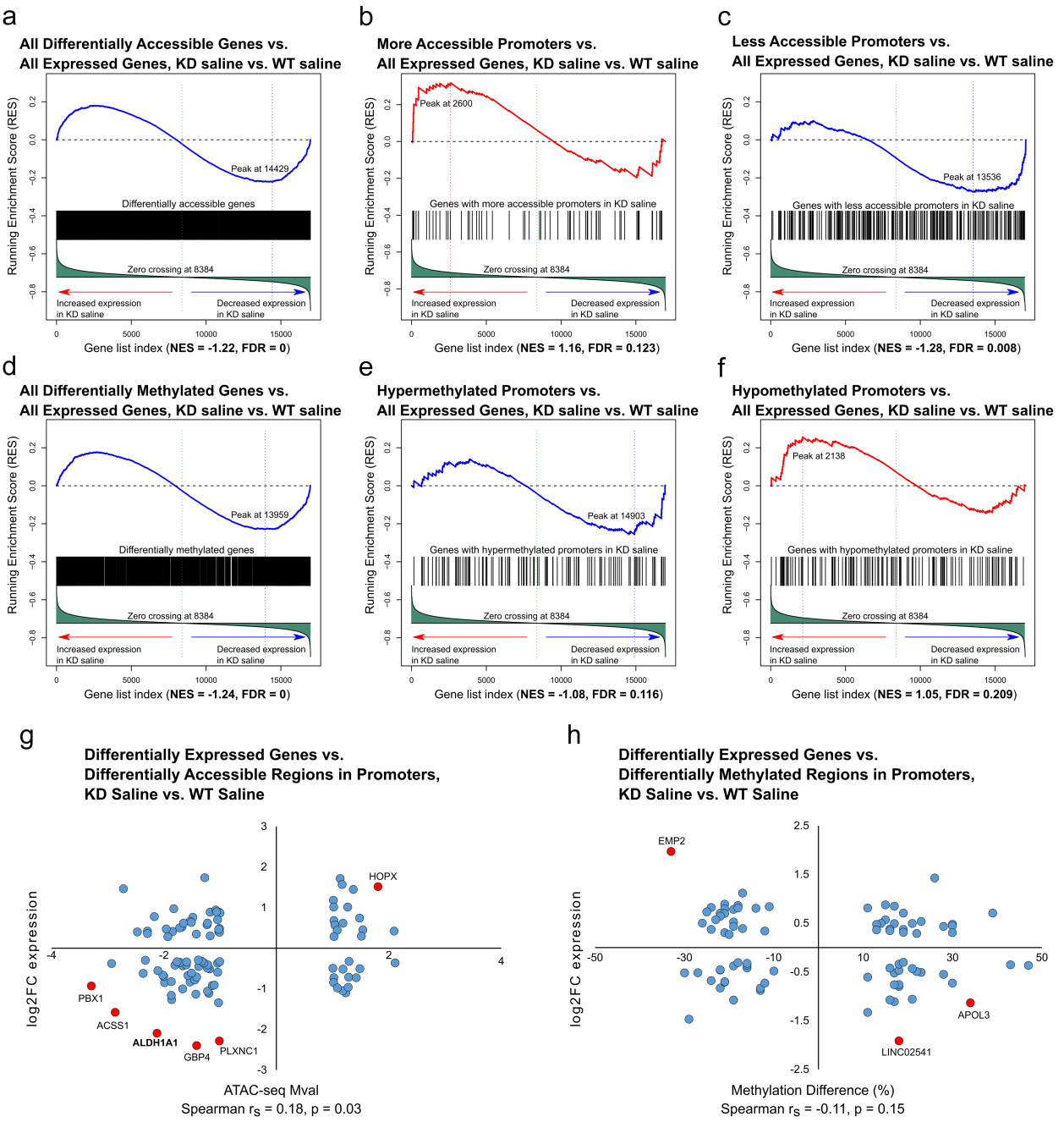

Figure 5. GSEAs reveal a correlation between changes in accessibility or DNA methylation and changes in gene expression.

The top of each plot shows the running enrichment score (ES), where a positive value indicates an enrichment for changes in either accessibility or methylation in genes that are increasing in gene expression, while a negative value indicates an enrichment for changes in either accessibility or methylation in genes that are decreasing in gene expression. The ES is the point of the largest deviation from zero in the upper portion of the plot. The normalized ES (NES) can be compared across gene sets. The FDR for the enrichment (based on a comparison with the gene set null distribution) is also shown. The following sets of genes were used as input to compare against gene expression changes (KD saline vs. WT saline comparison): (a) all changes in accessibility, (b) increased accessibility in promoters, (c) decreased accessibility in promoters, (d) all changes in methylation, (e) increased methylation in promoters, and (f) decreased methylation in promoters. The y-axis in both (g) and h) shows the log2 fold-change for DE genes, while the x-axis in (g) shows the ATAC-seq Mval (difference in mean signal intensity between the two conditions) and the x-axis in (h) shows the percent difference in methylation. Only genes that were DE and showed a change in accessibility or methylation at the promoter were included in (g) and (h), respectively. *P*-values were calculated using a right-tailed Spearman correlation coefficient test for (g) and a left-tailed Spearman correlation coefficient test for (h). Abbreviations: WT saline = *TET1* intact saline samples, KD saline = *TET1* knockdown saline samples.

Table 3). The top five most enriched pathways in genes associated with differentially accessible peaks following HDM treatment were all in the top 32 most enriched pathways following *TET1* knockdown. Additionally, all five of these pathways had the same inferred direction of change. Sixty-five (73.0%) enriched pathways following HDM treatment were also enriched following *TET1* knockdown, including TGF-β signalling and pulmonary fibrosis idiopathic signalling pathway (Supplementary Table 3). Of these 65, 55 had similar z-scores (i.e. the inferred direction of change in activation was the same), 8 had no activation z-scores calculated (due to limitations with how the pathways were constructed within IPA), and 2 had opposing activation z-scores. Collectively, our data show that HDM challenge and TET1 deficiency have similar impacts on chromatin accessibility in airway epithelial cells,

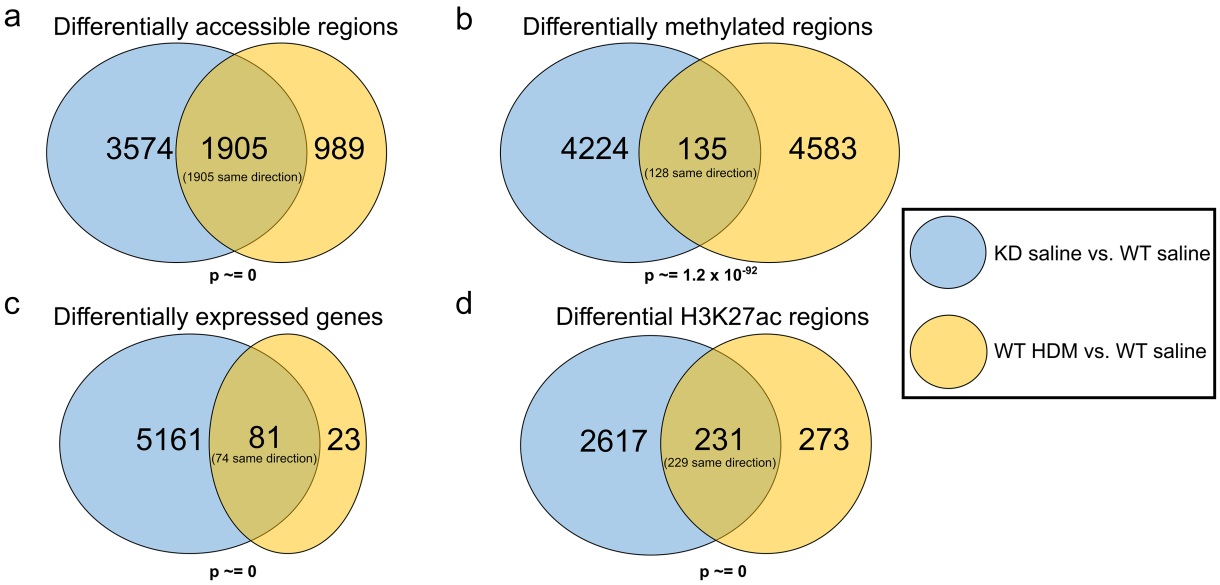

Figure 6. Overlap between changes following *TET1* knockdown and changes following HDM treatment.

Venn diagrams depicting the overlaps between changes in the KD saline vs. WT saline and the WT HDM vs. WT saline comparisons in (a) differentially accessible regions, (b) DMRs, (c) DE genes, and (d) differential H3K27ac regions. Changes in the 'same direction' refer to regions/genes that either increased in both comparisons or decreased in both comparisons. *P*-values were calculated using right-tailed Fisher's exact tests. Abbreviations: WT saline = *TET1* intact saline samples, WT HDM = *TET1* intact HDM samples, KD saline = *TET1* knockdown saline samples, KD HDM = *TET1* knockdown HDM samples.

with both likely impacting proinflammatory pathways and lung function.

HDM treatment led to DNA methylation changes that significantly overlap with those following *TET1* knockdown in HBECs

We previously showed that HDM challenges led to changes in 5mC and 5hmC in HBECs using microarrays, and changes in 5mC responsive to HDM and diesel particles significantly correlated with changes in gene expression [14]. When we compared methylation patterns between WT HDM and WT saline HBECs using WGBS, we identified 4718 significant DMRs (empirical *P*-value $\leq$ .01, at least 10% difference in methylation) annotated to 3428 unique genes (Supplementary Table 4). These DMRs were ~885 bp on average. Most DMRs were annotated to introns (43%), intergenic regions (37%), promoters (10%), or exons (7%). Compared to background regions, these DMRs were enriched for promoters, but depleted in introns (Supplementary Fig. 3). Of these DMRs, 48.8% were hypermethylated in WT HDM compared to WT saline (Fig. 1, Supplementary Fig. 5B). There were a small number but significantly more than expected positional overlaps between DMRs in the KD saline vs. WT saline comparison and DMRs in the WT HDM vs. WT saline comparison ($P = 1.2 \times 10^{-92}$, Fig. 6b). Despite such a small number of positional overlaps, methylation changed in the same way (i.e. increased or decreased) after either *TET1* knockdown or HDM treatment 94.8% of the time. These positional overlaps were annotated to genes such as *CLU*, *TLR7*, and *IL13RA1* (Supplementary Table 9). At the gene level, out of the genes that were associated with DMRs following *TET1* knockdown, 36.7% were also associated with at least one DMR following HDM treatment. The DMR-associated genes following HDM treatment were enriched for 70 IPA canonical pathways (FDR $\leq$ 0.05; Supplementary Table 5). These pathways were generally similar to enriched pathways from DMR-associated genes in the KD saline vs. WT saline comparison; there were six overlapping pathways in the top 10 enriched pathways from each comparison. Out of the enriched pathways from DMR-associated genes following *TET1* knockdown, 59.6% were also enriched in DMR-associated genes following HDM treatment, including pulmonary fibrosis idiopathic signalling pathway, nitric oxide signalling in the cardiovascular system, leukocyte extravasation signalling, and IL-8 signalling. Overall, HDM treatment and *TET1* knockdown had significantly overlapping effects on the methylome, potentially affecting genes and pathways contributing to inflammation and lung function.

HDM treatment led to few changes in expression, but these changes significantly overlap with *TET1* knockdown induced changes and were amplified by *TET1* knockdown

We next performed RNA-seq to assess the effect of HDM treatment on gene expression and to compare these results with how *TET1* knockdown affected gene expression. We identified 104 DE genes in the WT HDM vs. WT saline comparison (Supplementary Table 6). There were many fewer DE genes following HDM treatment alone compared to after *TET1* knockdown alone (104 vs. 5242 genes), 64.4% were upregulated following HDM treatment. Out of the 104 DE genes, 77.9% were also DE in the KD saline vs. WT saline comparison, indicating that most genes with changed expression following HDM treatment were also affected by *TET1* knockdown ($P = \sim 0$, Fig. 6c). Further supporting this notion was the finding that out of these shared DE genes, 91.4% changed in the same direction (i.e. HDM treatment and *TET1* knockdown both led to downregulation or both led to upregulation). These genes whose expression was altered similarly following HDM treatment or *TET1* knockdown included *IL1A* (increased), *IL1B* (increased), *IFNGR2* (increased), and *AHR* (decreased) (Supplementary Fig. 8A). We also performed IPA pathway analysis on the DE genes from the WT HDM vs. WT saline comparison to see if expression levels in similar pathways were affected by both HDM treatment and *TET1* knockdown (Fig. 3c, Supplementary Table 7). Of 22 enriched IPA pathways, 11 (50%) were also enriched in DE genes from the KD saline vs. WT saline comparison. Out of these 11 shared pathways,

7 had estimated activation z-scores in the WT HDM vs. WT saline comparison (Supplementary Fig. 8B); in all 7 cases, the activation z-scores for both comparisons indicated consistent pathway level changes. For example, the activation z-scores for AhR signalling were negative in both cases, indicating that expression changes following HDM treatment alone and *TET1* knockdown alone both likely led to some deactivation of that pathway. Importantly, HDM treatment had a much stronger impact on gene expression following *TET1* loss, as there were 1467 DE genes in the KD HDM vs. KD saline comparison (Supplementary Table 6, Supplementary Fig. 7). Of the 39 genes that were DE in WT HDM vs. WT saline and KD HDM vs. KD saline, 35 changed in the same direction following HDM treatment (Supplementary Fig. 7). Therefore, despite HDM treatment leading to fewer DE genes than knocking down *TET1* in HBECs, genes and pathways that were affected by HDM treatment were often affected by *TET1* knockdown, and *TET1* knockdown significantly amplified HDM-induced transcriptomic changes.

Loss of TET1 results in a transcriptomic signature enriched in stress and immune response following HDM challenges in HBECs

As our data demonstrated that TET1 loss tends to have a similar impact to HDM challenge on chromatin accessibility, DNA methylation, and gene expression, we next compared expression in KD HDM HBECs to WT HDM HBECs through RNA-seq analysis. In a pairwise analysis, we identified 4457 genes that were DE (FDR $\leq$ 0.05, FC $\geq$ 1.2, Fig. 1, Supplementary Table 6). Of these DE genes, 49.9% were significantly upregulated in KD HDM compared to WT HDM HEBCs (Fig. 1). The majority of these genes (67.6%) were also DE when comparing KD saline vs. WT saline. Out of the overlapping DE genes, 99% showed changes in the same direction when *TET1* was knocked down, suggesting that these gene expression changes were primarily driven by TET1 loss regardless of the presence of HDM (Supplementary Figs 4 and 5C). Pathway analysis via IPA on all DE genes from the KD HDM vs. WT HDM comparison (Fig. 3c, Supplementary Table 7) revealed the enrichment of 269 IPA pathways (FDR $\leq$ 0.05). These genes were enriched for pathways of interest such as oxidative phosphorylation, mitochondrial dysfunction, HIF1α signalling, NRF2-mediated oxidative stress response, and AhR signalling. Additionally, the significant enrichment and strong activation (activation z-score = 3.97) of EIF2 signalling in DE genes in KD HDM vs. WT HDM HBECs suggests an upregulation of protein translation. Interestingly, we also observed significant enrichment for genes involved in the regulation of cell cycle and division (cell cycle: G2/M DNA Damage Checkpoint Regulation, Cyclins and Cell Cycle Regulation; Cell Cycle: G1/S Checkpoint Regulation, etc.). Significant downregulation was observed in several cyclin and cyclin-dependent kinases (CCND1, CCND3, CDC25A, and CDK4/6) and transcriptional regulators required for E2F-mediated transcription (E2F6), which may block G1/S cycle progression, and this is similar to what we observed in KD saline compared to WT saline.

To further elucidate the role of TET1 in regulating responses to HDM, we separately analysed the 1444 genes that were DE in KD HDM vs. WT HDM, but not in KD saline vs. WT saline. There were several DE genes in this set that are subunits of the main complexes in the electron transport chain, including *ATP5F1C, ATP5MC1, COX5A, NDUFA4, NDUFA7, UQCR11*, and *UQCRQ*. There were also immune and detoxification genes such as *ARNT, FLOT2, GSTO2, JUN, JUNB, IL17RE, IRF2BP2, SMAD4, TLR5*, and *TRAF4* (examples shown in Supplementary Fig. 9). These genes were enriched for seven IPA pathways, including oxidative phosphorylation, mitochondrial dysfunction, and autophagy (Supplementary Table 10). All of these pathways were also enriched in the KD saline vs. WT saline DE genes (Supplementary Table 7) even though overlapping genes were specifically filtered out for this analysis, indicating that TET1 broadly regulates these pathways but that the specific genes that are impacted by the loss of *TET1* could be context-dependent.

The presence of HDM influences TET1's impact on chromatin accessibility and DNA methylation

In contrast to the mostly reduced accessibility observed in KD saline cells compare to WT saline cells, we observed a strong pattern of increased accessibility in KD HDM cells compared to WT HDM (Fig. 1). There were 6404 significantly different ATAC-seq peaks (Supplementary Table 2, annotated to 4449 unique genes), and 92.4% of the peaks showed increased peak intensity in KD HDM (Fig. 1). The differentially accessible peaks were 422 bp on average and were primarily annotated to introns (42.6%), intergenic regions (35.1%), promoters (9.2%), and exons (8.8%). Compared to background regions, these peaks were enriched in 5′ UTRs, exons, 3′ UTRs, and intergenic regions, while depleted in promoters (Supplementary Fig. 3). Of these genes associated with differential chromatin accessibility in KD HDM vs. WT HDM, 51.8% were also associated with differential accessibility in the KD saline vs. WT saline comparison. Only 10.5% of these overlapping genes, however, showed consistent changes in direction in the two comparisons. Out of the differentially accessible peaks in KD HDM vs. WT HDM, 30.8% overlapped positionally with a differentially accessible peak in KD saline vs. WT saline ($P = \sim 0$). For these positional overlaps, in only 1.4% did *TET1* knockdown have a consistent effect of either increasing or decreasing accessibility regardless of whether HDM was present or not. These results indicate a potential interaction between *TET1* knockdown and the presence of HDM since the effect of *TET1* knockdown was different depending on the environment. The presence of such an interaction could explain why, in a principal component analysis, PC1 (which explained 65.8% of the variance) separated WT saline and KD HDM samples from WT HDM and KD saline samples (Supplementary Fig. 6). Pathway analysis via IPA on genes associated with changes in accessibility revealed significant enrichment for 112 pathways (FDR $\leq$ 0.05; Supplementary Table 3), 61.6% of which also were enriched in significant ATAC peaks from KD saline vs. WT saline. Of the pathways where an activation z-score could be assigned (assuming a positive correlation between chromatin accessibility and gene expression), 96.8% showed opposite patterns of activation in KD HDM vs. WT HDM and KD saline vs. WT saline (Supplementary Fig. 8C). This indicates that knocking down *TET1* consistently leads to changes in chromatin accessibility in certain pathways, but that precisely how accessibility is affected might depend on whether HDM is present or not.

When we compared genome-wide DNA methylation levels in KD HDM samples to WT HDM samples, we identified 4086 DMRs (Fig. 1) annotated to 3037 unique genes (Supplementary Table 4). These DMRs were ~906 bp on average, and most of them were associated with either introns (42.8%), intergenic regions (36.2%), promoters (10.1%), or exons (7.2%). Compared to background regions, these DMRs were enriched in promoters, while depleted in introns (Supplementary Fig. 3). The 3037 DMR-associated genes were enriched for 68 IPA pathways (Fig. 3b, Supplementary Table 5). Of the genes that were associated with a DMR in this comparison (KD HDM vs. WT HDM), 34.4% were

also DMR-associated in the KD saline vs. WT saline comparison. Of these overlapping genes, the average methylation changes were in the same direction following *TET1* knockdown 49.4% of the time. There were 44 positional overlaps between KD HDM vs. WT HDM DMRs and KD saline vs. WT saline DMRs (more than expected by chance, $P = 6.5 \times 10^{-15}$). There were consistent directional changes in methylation regardless of whether HDM was present in 43.2% of these positional overlaps. These results imply that, similar to chromatin accessibility, methylation changes following *TET1* loss could have been influenced by the presence of HDM. There were only 10 positional overlaps between KD HDM vs. WT HDM DMRs and differentially accessible regions, adding another piece of evidence that the changes we observed in chromatin accessibility following *TET1* knockdown generally occurred in different regions of the genome than changes in DNA methylation.

Loss of *TET1* and HDM treatment led to significantly overlapping changes in H3K27ac, and these changes are enriched for asthma-associated changes in H3K27ac

Since H3K27ac is highly enriched at active enhancers [64] whose presence can be significantly influenced by chromatin accessibility, we performed H3K27ac ChIP-seq and searched for regions with changes in H3K27ac signal intensity. We identified 2848 differential regions in which KD saline and WT saline groups both had some H3K27ac signal, with only 16 regions showing increased H3K27ac in KD saline and 2832 regions showing decreased H3K27ac in KD saline (Supplementary Table 11). Out of these 2848 regions, 34.2% were annotated to a DE gene, of which 57.1% showed the generally expected positive correlation between H3K27ac levels and expression (enriched pathways in Supplementary Table 12). Interestingly, 33 of these differences overlapped positionally with changes in chromatin accessibility ($P = .03$, Fig. 7a), including an overlap at *MAP3K14* (Fig. 2b), which stimulates NFKB signalling [65].

As enhancers may cluster together and form super-enhancers to drive transcription of genes implicated in disease [51, 66], we next compared the presence of super-enhancers in KD saline vs. WT saline samples. We identified 109 consensus 'gained' super-enhancers in KD saline samples that did not overlap with any consensus super-enhancers in WT saline samples, and 329 'lost' consensus super-enhancers in WT saline samples with no overlaps in the KD saline group (Supplementary Table 13). These 438 'gained' or 'lost' super-enhancer regions overlapped with 140 DE genes (i.e. the closest gene to the super-enhancer was DE) and 146 overlapped physically with regions with changes in chromatin accessibility ($P = 1.75 \times 10^{-62}$, Fig. 7a). A positive correlation between 'gain' or 'loss' of a nearby super-enhancer and changes in expression might be generally expected, but we observed this expected correlation only 41.4% of the time. Overall, we generally observed decreased H3K27ac signal in KD saline samples compared to WT saline samples, but these changes were not well correlated with changes in gene expression, possibly because other regulatory changes were underlying gene expression changes, changes in expression came after the time point that we sampled, or our 'nearest gene' annotation strategy might not always connect a regulatory region to its affected gene.

Similar to what we observed following *TET1* knockdown, a majority of regions with significant differences in H3K27ac showed decreased levels in WT HDM compared to WT saline (374/504, 74.2%) (Supplementary Table 11). These changes in H3K27ac overlapped with nine DE genes, and there was a positive correlation between changes in H3K27ac and gene expression in seven of these instances (77.8%). These regions largely overlapped with differential H3K27ac regions from the KD saline vs. WT saline comparison ($P = \sim 0$, Fig. 6d). Also similar to what we observed following *TET1* knockdown, there were many more 'lost' super-enhancers in WT HDM (329) than 'gained' super-enhancers [44] in WT HDM (Supplementary Table 13). These 415 'gained' or 'lost' super-enhancer regions overlapped with only 4 DE genes (there were only 104 DE genes in WT HDM vs. WT saline in total), and in only 1 out of these 4 DE genes did we observe a positive correlation between super-enhancer presence and expression changes. When comparing KD HDM to WT HDM, out of 1479 regions showing significant changes in H3K27ac in regions where both groups had H3K27ac signal, 99.4% showed decreased levels of H3K27ac in KD HDM (Supplementary Table 11). There were 482 of these regions with significant differences in H3K27ac that overlapped with a significant DE gene, and 67% showed a positive correlation with changes in expression. However, unlike what we observed following *TET1* knockdown and HDM treatment alone (both led to many more 'lost' super-enhancers based on analysis of H3K27ac ChIP-seq), the number of 'lost' super-enhancers (194) was similar to the number of 'gained' super-enhancers (226) in KD HDM (Supplementary Table 13). These 420 'gained' or 'lost' super-enhancer regions overlapped with 116 DE genes (there were only 104 DE genes in WT HDM vs. WT saline in total), but only 47.4% of the time did we observe a positive correlation between super-enhancer presence and expression changes. These super-enhancer results provide another example of the combination of *TET1* knockdown and HDM treatment potentially having an interactive effect on epigenomic regulation. Similar to the results from KD saline vs. WT saline, there was only limited correlation between super-enhancer gain or loss and expression, but there was some correlation between changes in H3K27ac levels and expression. Overall, this indicates that *TET1* knockdown and HDM treatment both lead to similar decreases in H3K27ac presence, again highlighting that these two conditions have a similar impact on the overall regulatory landscape.

Besides enhancer-specific markers, we also observed significant overlap between TET1-regulated differentially accessible regions and all A549 ENCODE [26] predicted cCREs (defined by chromatin accessibility, CTCF binding, H3K27ac, and H3K4me3) and CTCF-bound cCREs (Fig. 7a). As CTCF is important in setting up 3D chromatin interactions and TADs, we also quantified the overlap between differentially accessible regions and TADs in A549 cells (GSE92819) and found significant overlap (Fig. 7a). In addition, evidence from mouse model and HBECs support a protective role of TET1 against allergic asthma, which could be due to its role in promoting AhR signalling and limiting the expression of pro-inflammatory cytokines [9, 67]. Therefore, we searched for the presence of asthma-associated variations in histone acetylation [51] and DNA methylation found in airway epithelial cells [52–55] among TET1-loss induced differentially accessible regions and DMRs. We observed significant enrichment for asthma-associated H3K27ac changes and asthma or allergy-associated DMRs or DMPs [52, 55] only among TET1-loss induced differentially accessible regions (Fig. 7a and b), further supporting the relevance of TET1's regulation of chromatin accessibility in asthma. Therefore, our data support that TET1-mediated chromatin accessibility might influence H3K27ac marks, *cis*-regulatory elements, and CTCF binding to regulate gene expression, which may explain its role in protection from inflammation and asthma.

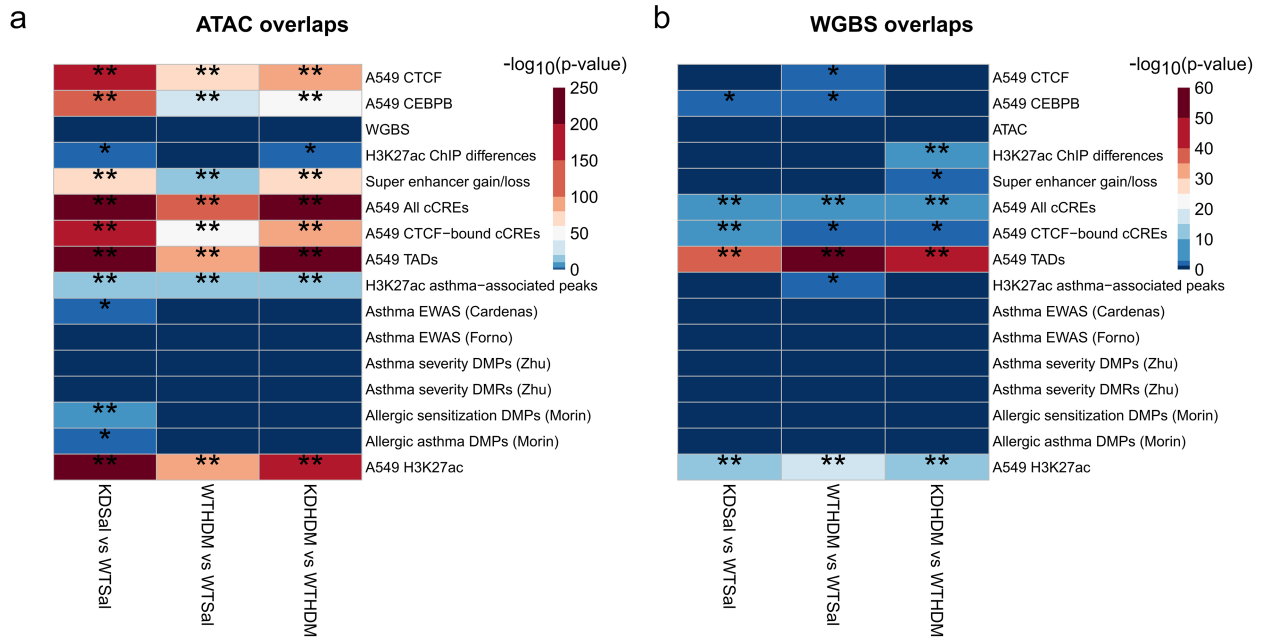

Figure 7. Overlap significance between our data and public datasets of interest.

Significance of overlaps between various genomic regions of interest with (a) our ATAC-seq (chromatin accessibility) peaks and (b) our WGBS (methylation) DMRs. The following labels refer to data from the current study: 'WGBS', 'ATAC', 'H3K27ac ChIP-differences', and 'Super-enhancer gain/loss'. 'A549 CTCF' (GSM1003606), 'A549 CEBPB' (GSM935630), 'A549 TADs' (GSE92819), and 'A549 H3K27ac' (GSE118840) refer to data retrieved from the NCBI GEO. 'A549 All cCREs' and 'A549 CTCF-bound cCREs' refer to cCREs downloaded from https://screen.encodeproject.org/. The rest of the data were retrieved from the following sources (first author's last name is in parentheses): 'H3K27ac asthma-associated peaks (McErlean)' [51], 'Asthma EWAS (Cardenas)' [52], 'Asthma EWAS (Forno)' [53], 'Asthma severity DMPs (Zhu)' [54], 'Asthma severity DMRs (Zhu)' [54], and 'Allergic sensitization DMPs (Morin)', [55] and 'Allergic asthma DMPs (Morin)' [55]. * = significant by *P*-value (<.05), ** = significant by Bonferroni corrected *P*-value (<.0012). Abbreviations: WT saline = *TET1* intact saline samples, WT HDM = *TET1* intact HDM samples, KD saline = *TET1* knockdown saline samples, KD HDM = *TET1* knockdown HDM samples.

Altered chromatin accessibility following loss of *TET1* and HDM treatment may affect CTCF and CEBP binding

As altered chromatin accessibility may impact the binding of TFs and therefore lead to changes in gene expression, we next performed unbiased HOMER and RELI TF enrichment analyses. Using a custom HOMER database of all human TF-binding motifs obtained from the CisBP database [32] (see Methods), we compared TF-binding motif enrichment in peaks that had changed accessibility following *TET1* KD with peaks that did not show any significant change in accessibility (Fig. 8). We also performed a similar analysis with RELI, which utilizes results from publicly available ChIP-seq experiments instead of TF-binding motifs (Fig. 8). In regions where KD saline had reduced accessibility, both analyses indicated lower enrichment of CTCF- and CEBP-binding sites compared to regions that were not changing in accessibility (Fig. 8). In regions where KD saline had increased accessibility, however, both analyses showed increased enrichment of CEBP-binding sites and reduced enrichment of CTCF-binding sites. Similar patterns were observed in regions with differential accessibility following HDM challenges. Relative depletion of CTCF-binding sites was also observed in regions where KD HDM had increased accessibility in both the HOMER and RELI analyses. In contrast, we observed no enrichment for either CTCF- or CEBP-binding sites within DMRs (Supplementary Fig. 10). These data suggest the *TET1*-regulated chromatin accessibility may specifically impact CTCF and CEBP binding, in a similar way to HDM-induced changes.

In order to further test the association between CTCF and CEBP binding and changes in chromatin accessibility, we compared binding sites for CTCF (GSM1003606) and CEBPB (GSM935630) in A549 cells to our differentially accessible peaks. The differentially accessible peaks overlapped much more frequently than expected by chance with the CTCF peaks (Fig. 7a). DMRs between KD saline HBECs and WT saline HBECs, however, did not overlap more frequently than expected with the CTCF-binding sites from A549 cells (Fig. 7b), emphasizing how the loss of TET1 likely affects gene regulation in different ways in different types of genomic environment. There was also significant overlap between both differentially accessible peaks (Fig. 7a) and DMRs (Fig. 7b) and CEBPB-binding sites in A549 cells. The much lower *P*-value and much greater odds ratio for the differentially accessible peaks, however, imply a more significant overlap between differentially accessible peaks and CEBPB sites than between DMRs and CEBPB sites. Therefore, these data support that TET1-associated changes in accessibility have a bigger impact on CTCF and CEBPB binding than TET1-associated changes in DNA methylation in airway epithelial cells.

A TET1-mediated regulatory element at the *IL1B* locus enhances gene expression

HDM and TET1 loss both activate the acute phase response pathway and downregulate the AHR signalling pathway (Supplementary Fig. 8B). *IL1B*, a major stimulator of the acute phase response pathway [68] that has been linked to asthma [69], showed increased gene expression following both TET1 loss and HDM treatment (Supplementary Fig. 8A by RNA-seq and Fig. 9a by RT-qPCR from a validation experiment). Interestingly, a region downstream of *IL1B* became significantly less accessible following HDM treatment and became significantly more accessible in KD HDM compared to WT HDM. This region overlapped with a predicted cCRE from A549 ENCODE data (Fig. 9b). Reporter assays

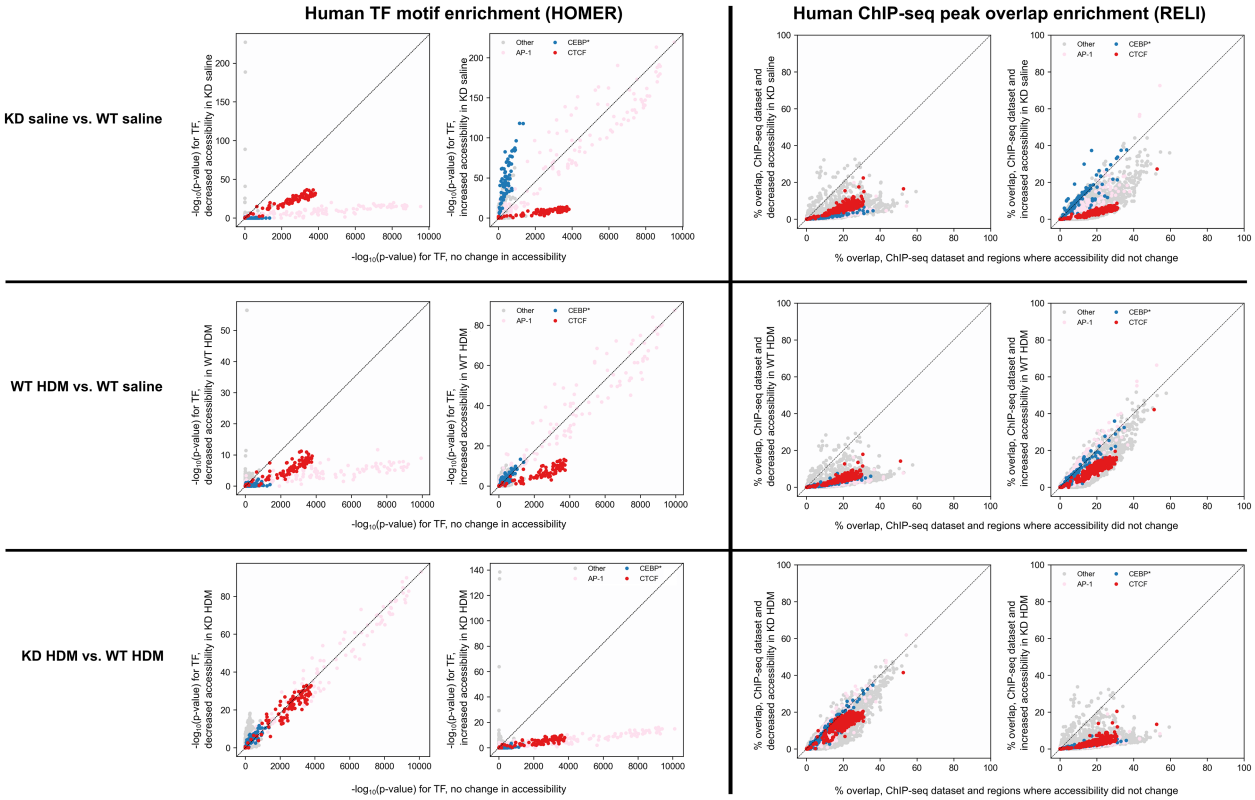

Figure 8. Comparison of TF-binding enrichment results in differentially accessible ATAC-seq peaks vs. unchanged ATAC-seq peaks.

The left set of panels shows results for TF motif enrichment analyses (HOMER). The right set of panels shows results for ChIP-seq peak enrichment analyses (RELI). Each dot represents a human TF-binding site motif (left set of panels) or ChIP-seq dataset (right set of panels). In all panels, the x-axes indicate enrichment (–log *P*-values) for regions with equivalent accessibility between the two conditions (i.e. statistically equivalent ATAC-seq peaks). Likewise, in all panels, the y-axes show the enrichment for a given ATAC-seq dataset in regions with altered accessibility (i.e. differential ATAC-seq peaks). The x- and y-axes have been scaled to enable direct comparison of the rank order of the *P*-values. The axes do not have the same scale because the *P*-values are strongly influenced by the number of peaks (more peaks lead to globally stronger *P*-values). For each pair of panels, gains in accessibility are shown on the left y-axis, and losses in accessibility are shown on the right y-axis. Motifs are color-coded by the TF family (see keys). For each panel, points straying from the diagonal line indicate a difference in enrichment between the two compared ATAC-seq regions (e.g. TF motifs more strongly enriched in opened vs. unaltered ATAC-seq peaks). Abbreviations: WT saline = *TET1* intact saline samples, WT HDM = *TET1* intact HDM samples, KD saline = *TET1* knockdown saline samples, KD HDM = *TET1* knockdown HDM samples.

confirm that this region enhances the expression of a florescence gene reporter gene at baseline (Fig. 9c). These data further support that TET1 may regulate chromatin accessibility and enhancer activity to control gene expression and response to allergen in HBECs.

Discussion

In this study, we assessed how knockdown of *TET1* gene expression and challenge of HBECs with HDM extract (known for its causal role in allergic asthma [63]) affected chromatin accessibility, H3K27ac levels, DNA methylation, and gene expression. One of our most striking findings was how HDM treatment and TET1 status led to highly specific changes in chromatin accessibility. When *TET1* was knocked down or when cells were treated with HDM without knocking down *TET1*, chromatin tended to lose more often than gain accessibility. When *TET1* was knocked down and cells were treated with HDM, however, chromatin was generally more accessible. Importantly, a significant portion of chromatin changes resulting from *TET1* loss overlapped with chromatin changes following HDM challenges. There was also significant overlap between the effects of HDM treatment and *TET1* loss on DNA methylation and H3K27ac levels. Despite the relatively small number of DE genes following HDM treatment alone ($N = 104$), 74 DE genes changed in the same direction in TET1 KD HBECs, and many more genes had significant changes following HDM challenges in TET1 KD HEBCs ($N = 1467$). Overall, *TET1* knockdown and HDM treatment in HBECs had a significantly overlapping effect on the epigenome. *TET1* knockdown amplified transcriptomic changes in response to HDM and modified many asthma-related genes and pathways, reinforcing results from our previous studies indicating that TET1 plays a protective role in allergic asthma [9, 67].

TET1-mediated changes in chromatin accessibility rarely overlap with TET1-mediated changes in DNA methylation and may represent separate modes of gene regulation

TET proteins regulate gene expression and cellular function via two main mechanisms: (i) catalytic activity-dependent promotion of DNA demethylation [70] and (ii) catalytic activity-independent mechanisms to modify histone marks [71–74]. The catalytic activity of TET proteins converts 5mC to 5hmC and eventually results in the removal of DNA methylation [11]. It has also been reported that 5mC disrupts CTCF binding [58, 59], while CEBP prefers to bind 5mC compared to 5hmC [75]. Therefore, if the enzymatic activity of TET1 plays a major role in HBEC, we would expect to see increased 5mC and decreased 5hmC resulting in increased DNA methylation [76, 77], reduced CTCF binding, and increased CEBP binding in *TET1* KD HBECs. Unexpectedly, we observed nearly equal numbers of significantly hypermethylated and hypomethylated regions and no enrichment for either CTCF- or CEBP-binding

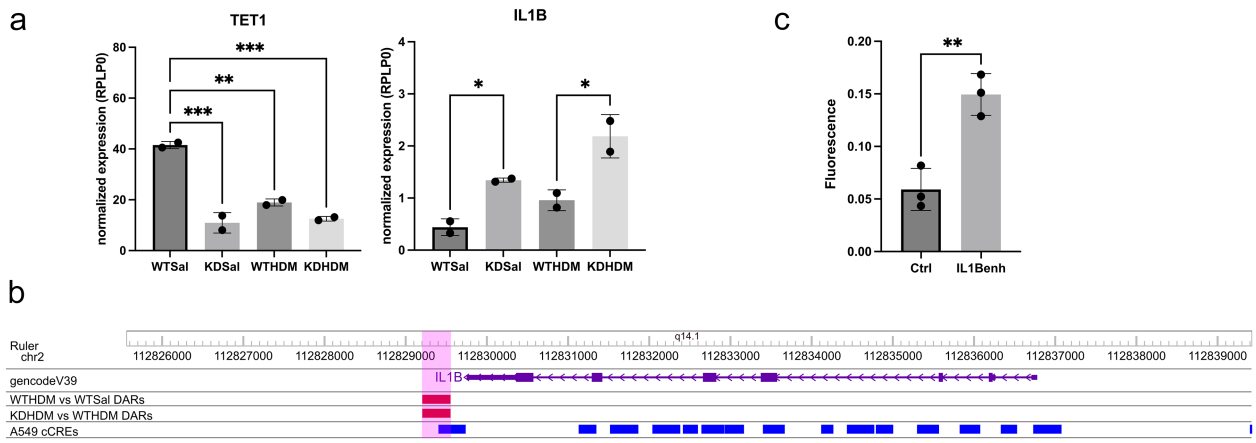

Figure 9. Impact of Tet1 on IL1B expression and identification of a Tet1-regulated enhancer.

(a) Loss of Tet1-enhanced expression of IL1B in HBECs. ANOVA test with multiple testing correction was performed. *$P < .05$, **$P < .01$, ***$P < .005$. (b) Changes in chromatin accessibility following HDM treatment near *IL1B* overlap with a cCRE in A549 cells. (c) Changes in expression following introduction of an plasmid containing candidate *IL1B* enhancer. The shaded region in (b) shows a region that was differentially accessible in WT HDM vs. WT saline and in KD HDM vs. WT HDM (decreased in WT HDM in both cases). 'A549 cCREs' refer to cCREs downloaded from https://screen.encodeproject.org/. Abbreviations: WTHDM = *TET1* intact HDM samples, WTSal = *TET1* intact saline samples, KDHDM = *TET1* knockdown HDM samples, DARs = differentially accessible regions, Ctrl = control reporter plasmid containing minimal CMV promoter, IL1Benh = plasmid containing candidate *IL1B* enhancer and minimal CMV promoter.

sites within DMRs (Supplementary Fig. 10). However, we observed a lack of CTCF and enrichment of CEBP-binding sites in regions with changes in chromatin accessibility, which significantly overlapped with regions with H3K27ac changes and had only few overlaps with DMRs. Additionally, while DMRs in all comparisons were significantly enriched in promoters compared to background regions, differentially accessible regions were significantly depleted in promoters compared to background regions. These data collectively suggest that the catalytic activity-independent function of TET1 is primarily responsible for the changes in chromatin accessibility and histone marks. Several known histone modifying enzymes were reported to interact with TET1, such as EZH2 [72, 78–81] and SIN3A [82, 83], whose interaction with TET1 in HBECs will be examined in future studies. One caveat is that WGBS measures the sum of 5mC and 5hmC and cannot distinguish between these two modifications [61]. Therefore, our study may have missed regions with simultaneous opposite significant changes (e.g. increased 5mC and decreased 5hmC). Additionally, the changes in other epigenetic mechanisms may indirectly influence DNA methylation. Indeed, ∼50% of changes in chromatin accessibly occurred within gene bodies, which are normally highly methylated. Therefore, the two functions of TET1 protein regulation may coordinate to influence the epigenetic landscape and regulate gene expression. Future studies using emerging technologies such as nanopore sequencing that can separately identify 5mC and 5hmC will be needed to further delineate the relationship between TET1-mediated changes in DNA methylation, histone modifications, TF binding and chromatin accessibility.

TET1 loss-induced expression changes in AhR signalling genes may promote allergen-induced inflammation

We previously showed that TET1 positively regulates the expression of several genes in the AhR signalling pathway at baseline and following HDM challenges in mice [9]. This suggests a mechanistic explanation for the exacerbated asthma-like phenotype in TET1-deficient mice following HDM treatment. In our current study in HBECs, DE genes in KD saline vs. WT saline and KD HDM vs. WT HDM were both enriched for the AhR signalling pathway. Overlapping DE genes for these comparisons included *AHR*, *ALDH1A1*, *CYP1B1*, *GSTO1*, and *IL1B*. The activation z-scores for the AhR signalling pathway were negative for both comparisons, implying that loss of TET1 leads to lower activation of this pathway. The evidence for deactivation, however, was much stronger in the presence of HDM (activation z-scores: −1.81 for KD HDM vs. WT HDM, −0.51 for KD saline vs. WT saline). These *in vitro* HBEC results for genes involved in AhR signalling were generally consistent with the aforementioned *in vivo* mouse study results, further supporting the role of TET1 in regulating this pathway, especially following HDM challenges. Several DE genes in the AhR signalling pathway had changes in accessibility and/or methylation when *TET1* was knocked down (including *AHR*, *ALDH1A1*, and *NFE2L2* in KD saline vs. WT saline and *ALDH1A1*, *MGST1*, and *CYP3A5* in KD HDM vs. WT HDM). *ALDH1A1* in particular had decreased accessibility at the promoter and decreased expression in KD saline vs. WT saline. In addition, the AhR signalling pathway was also enriched in regions with differences in H3K27ac in KD saline vs. WT saline and KD HDM vs. WT HDM. Assuming a general positive correlation between H3K27ac presence and gene expression, changes in H3K27ac were predicted to reduce the activity of this pathway (activation z-scores: −2.07 for KD saline vs. WT saline, −2.83 for KD HDM vs. WT HDM). Importantly, changes in chromatin accessibility, as well as other epigenetic modifications, following stimulus do not necessarily correlate with immediate changes in gene expression. For example, in other studies, short-term IL-1α treatment led to changes in chromatin accessibility, but the majority of those changes were not correlated with changes in gene expression [59, 84]. In our study, however, we noted a significant positive relationship between significant changes in accessibility at the promoter and gene expression in DE genes in the KD saline vs. WT saline comparison. Additionally, for this comparison, DE genes with increased accessibility at their promoters had a positive average change in expression, while DE genes with decreased accessibility at their promoters had a negative average change in expression. Nevertheless, although overall gene expression programs differ, the chromatin state in KD saline resembles HDM-treated HBECs, suggesting a pro-inflammatory chromatin state created by TET1 loss that may promote the response to HDM. In

support of this, we only observed a trend of increased expression in *IL33* (a gene known to contribute to airway inflammation following environmental exposures [85]) in WT HDM vs. WT saline, but this gene was significantly upregulated in KD HDM vs. WT HDM.

Combining *TET1* knockdown and HDM treatment led to unique changes in the epigenome, which may influence enhancer activity and contribute to more substantial proinflammatory effects

TET1 knockdown and HDM treatment have each individually been linked to asthma [9, 63]. These two treatments generally led to very similar changes in accessibility and some similar changes in methylation (significantly more overlap than expected by chance, and a high level of concordance in the direction of change). However, in the KD HDM vs. WT HDM comparison, we observed generally increased accessibility in the KD HDM group, which was the opposite of what we observed in KD saline vs. WT saline and WT HDM vs. WT saline. KD HDM samples were closest to WT saline samples in a principal component analysis of the chromatin accessibility data, indicating that combining *TET1* knockdown with HDM treatment might have reverted some of the changes in accessibility linked to *TET1* knockdown alone. While the epigenetic changes following *TET1* knockdown were potentially affected by HDM presence, *TET1* knockdown seemingly had a more consistent effect on gene expression. Out of 4457 DE genes in KD HDM vs. WT HDM, 3013 (67.6%) were also DE in KD saline vs. WT saline. Out of these overlapping DE genes, 99% showed consistent changes in direction when *TET1* was knocked down. There were still, however, 1444 genes that were DE in KD HDM vs. WT HDM and not in KD saline vs. WT saline, suggesting that the combination of HDM treatment and *TET1* knockdown might have some unique effects on the transcriptome.

One chromatin mark that showed general correlation with expression in both KD HDM vs. WT HDM and KD saline vs. WT saline was H3K27ac, a marker for enhancers [64]. A previous study found 4321 regions showing differential levels of H3K27ac between asthmatic and healthy bronchial epithelial cells [51], indicating that changes in this chromatin mark could have some link to asthma. Indeed, regions with changing H3K27ac in both KD saline vs. WT saline and KD HDM vs. WT HDM were both enriched for genes in the AhR signalling pathway, a pathway that was inhibited in Tet1-deficient mice when exposed to HDM [9] and known to regulate airway inflammation [86]. We also observed changes in H3K27ac peaks at or close to some regions whose chromatin accessibility was regulated by TET1 and HDM in HBECs (Fig. 2b). In addition, computational analysis predicted reduced CTCF binding at these regions. CTCF is a well-established regulator of chromatin looping (long distance chromatin interactions) [87–89]. Chromatin folding/looping allows regulatory gene elements to act on their targets located long distances away (*in trans*) [90]. Allele-specific chromatin remodelling mediated by CTCF was linked to differential expression of genes in the 17q12-q21 locus, which has been linked to childhood-onset asthma [91]. In our datasets, we observed significant enrichment for CTCF-binding sites, CTCF-bound cCREs, TADs, and H3K27ac peaks in A549 cells at regions with TET1- and HDM-mediated chromatin accessible changes. Taken together, future studies should assess the effects of other histone modifications, CTCF binding, and enhancer function following TET1 loss. Functional studies directly assessing the interplay between TET1, histone modifications, CTCF binding, and gene expression could prove fruitful for understanding the role of TET1 in responding to environmental exposures and regulating asthma.

Study limitations and future directions

This study had some limitations. The sample size for each analysis was relatively small, so we used both stringent quality control and significance cut-offs (e.g. we required at least two-fold change for a significant difference in accessibility). By using these stringent cut-offs, however, we likely missed biologically relevant changes in some genes/regions; however, this approach was deemed necessary to limit false positives. Another limitation was that all HBEC samples were collected at only one time point (after 48 h of siRNA with 24 h of treatment with either saline or HDM). Differences in timing for changes in different epigenetic modifications and gene expression to occur, as well as the presence of other gene-specific regulatory mechanisms, might explain, for example, why ~74% of DE genes in KD saline vs. WT saline were not associated with DMRs or differentially accessible regions. Another potential reason for this lack of correlation was our strategy of annotating regions of interest (e.g. DMRs or differentially accessible regions) using the closest gene. We likely missed *trans*-regulatory interactions correlated with gene expression changes because of this. Recent studies utilizing promoter capture Hi-C to annotate functional elements outside promoters to target genes showed great promise in understanding asthma-associated genetic and epigenetic variants [55, 92]. Future studies should include measurements at a variety of time points to enable a more comprehensive understanding of epigenetic regulation of gene expression following *TET1* knockdown and HDM treatment in primary airway epithelial cells and utilize function-informed gene annotation. Another limitation was that WGBS measures the sum of 5mC and 5hmC and cannot differentiate between 5mC and 5hmC [61], so any effect that *TET1* knockdown had on 5mC and 5hmC individual levels was not captured in this study. Additionally, *TET1* knockdown altered the expression of other epigenetic modifying proteins such as DNMT1, histone deacetylase, and demethylases. As this siRNA does not have any targets except the *TET1* transcript predicted by NCBI BLASTN, we speculate that the altered expression of these genes is an indirect effect of *TET1* knockdown. We also observed a similar impact of *Tet1* knockout on *Dnmt1* and *Dnmt3b in vivo* [9]. It is possible that the changes observed from *TET1* siRNA treatment in this study were due to the collective dysregulation of multiple epigenetic processes. Future experiments will be designed to investigate the co-ordination of epigenetic players in the airway epithelial cells. Lastly, there were several other epigenetic changes that likely affected gene expression. For example, TET1 can directly interact with TFs and histone modification enzymes [15], so it would be worthwhile to directly measure where Tet1 protein binds and how histone modifications and TF binding change following *TET1* knockdown. Collectively, our analyses reveal a new link between TET1, CTCF, and enhancers that future studies should expand on to improve our understanding of the role of TET1 in responding to environmental exposures linked to asthma and other lung diseases.

Conclusions

Our genome-scale data analyses indicate that acute reduction of *TET1* expression, a key regulator of asthma, in HBECs leads to global changes in chromatin accessibility, DNA methylation, H3K27ac, and gene expression. These changes significantly overlap with changes observed following HDM challenge, a direct

cause of allergic asthma development, modify genes and pathways implicated in asthma, and may explain the amplified transcriptomic responses in *TET1*-deficient cells to HDM. Altered chromatin accessibility following loss of *TET1* expression was found to potentially affect the binding of CTCF and CEBP and enhancer activities. Little overlap was observed between regions of the genome that experienced TET1-induced changes in chromatin accessibility and DNA methylation, supporting a multifaceted gene regulatory role of TET1. Overall, our data shed light on how TET1 regulates critical pathways involved in asthma and response to allergens.

Author contributions

H.J. conceived the study; A.P.B performed data analysis of RNA-seq and WGBS and integrated analysis of these datasets with ATAC-seq; S.P. performed analysis of ATAC-seq datasets under the supervision of M.T.W. and generated RELI and HOMER results; L.C., S.E., and C.P. completed the cell culture work; L.C. generated ATAC-seq and H3K27ac libraries and submitted samples for WGBS and RNA-seq analysis; A.B. assisted in ChIP-seq experiment and data analysis; A.P.B. drafted and edited the manuscript; A.B., M.T.W., and H.J. edited the manuscript. All authors reviewed the manuscript.

Supplementary data

Supplementary data is available at *EnvEpig* online.

Conflict of interest: Artem Barski is a co-founder of Datirium, LLC (a developer of https://SciDAP.com

NGS data analysis platform) and a member of Scientific Advisory Board of LDRTC, LLC.

Funding

The sequencing was carried out at the DNA Technologies and Expression Analysis Cores of the UC Davis Genome Center, supported by NIH Shared Instrumentation Grant 1S10OD010786-01. This work was supported by NIH/NIAID R01AI141569 (H.J.); and NIH/NIAID U01AI150748, NIH/NIAMS P30AR070549, and CCHRF ARC Award #53632 (M.T.W.). H.J. was also supported by NIH/NIEHS P30ES023513-supported EHSC scholar fund and UC Davis Faculty Startup fund.

Data availability

ATAC-seq, WGBS, and RNA-seq data have been deposited in the Gene Expression Omnibus (GEO, accession numbers GSE293175, GSE293176, GSE293178). The code used for analyses can be found at https://github.com/davisjilab/HBECmultiomics.

References

1. Nunes C, Pereira AM, Morais-Almeida M. Asthma costs and social impact. *Asthma Res Pract* 2017;**3**:1.
2. Weiss ST, Raby BA, Rogers A. Asthma genetics and genomics 2009. *Curr Opin Genet Dev* 2009;**19**:279–82.
3. Nurmagambetov T, Kuwahara R, Garbe P. The economic burden of asthma in the United States, 2008-2013. *Ann Am Thorac Soc* 2018;**15**:348–56.
4. Somineni HK, Zhang X, Biagini Myers JM *et al.* Ten-eleven translocation 1 (TET1) methylation is associated with childhood asthma and traffic-related air pollution. *J Allergy Clin Immunol* 2016;**137**:797–805e5.
5. Kabesch M, Tost J. Recent findings in the genetics and epigenetics of asthma and allergy. *Semin Immunopathol* 2020;**42**:43–60.
6. Reese SE, Xu C-J, den Dekker HT *et al.* Epigenome-wide meta-analysis of DNA methylation and childhood asthma. *J Allergy Clin Immunol* 2019;**143**:2062–74.
7. Zhang X, Biagini Myers JM, Burleson JD *et al.* Nasal DNA methylation is associated with childhood asthma. *Epigenomics* 2018;**10**:629–41.
8. Ji H, Biagini Myers JM, Brandt EB *et al.* Air pollution, epigenetics, and asthma. *Allergy Asthma Clin Immunol* 2016;**12**:51.
9. Burleson JD, Siniard D, Yadagiri VK *et al.* TET1 contributes to allergic airway inflammation and regulates interferon and aryl hydrocarbon receptor signaling pathways in bronchial epithelial cells. *Sci Rep* 2019;**9**:7361.
10. Pastor WA, Aravind L, Rao A. TETonic shift: biological roles of TET proteins in DNA demethylation and transcription. *Nat Rev Mol Cell Biol* 2013;**14**:341–56.
11. Weber AR, Krawczyk C, Robertson AB *et al.* Biochemical reconstitution of TET1–TDG–BER-dependent active DNA demethylation reveals a highly coordinated mechanism. *Nat Commun* 2016;**7**:10806.
12. Yeung BHY, Huang J, An SS *et al.* Role of isocitrate dehydrogenase 2 on DNA hydroxymethylation in human airway smooth muscle cells. *Am J Respir Cell Mol Biol* 2020;**63**:36–45.
13. Li H, Lu T, Sun W *et al.* Ten-eleven translocation (TET) enzymes modulate the activation of dendritic cells in allergic rhinitis. *Front Immunol* 2019;**10**:2271.
14. Zhang X, Chen X, Weirauch MT *et al.* Diesel exhaust and house dust mite allergen lead to common changes in the airway methylome and hydroxymethylome. *Environ Epigenet* 2018;**4**:dvy020.
15. Zhu T, Brown AP, Ji H. The emerging role of ten-eleven translocation 1 in epigenetic responses to environmental exposures. *Epigenet Insights* 2020;**13**:2516865720910155.
16. Veazey KJ, Wang H, Bedi YS *et al.* Disconnect between alcohol-induced alterations in chromatin structure and gene transcription in a mouse embryonic stem cell model of exposure. *Alcohol* 2017;**60**:121–33.
17. Feng J, Shao N, Szulwach KE *et al.* Role of Tet1 and 5-hydroxymethylcytosine in cocaine action. *Nat Neurosci* 2015;**18**:536–44.
18. Chaudhry MA, Omaruddin RA. Differential DNA methylation alterations in radiation-sensitive and -resistant cells. *DNA Cell Biol* 2012;**31**:908–16.
19. Hirao-Suzuki M, Takeda S, Sakai G *et al.* Cadmium-stimulated invasion of rat liver cells during malignant transformation: evidence of the involvement of oxidative stress/TET1-sensitive machinery. *Toxicology* 2021;**447**:152631.
20. Sun Z, Xu X, He J *et al.* EGR1 recruits TET1 to shape the brain methylome during development and upon neuronal activity. *Nat Commun* 2019;**10**:3892.
21. Zhong J, Li X, Cai W *et al.* TET1 modulates H4K16 acetylation by controlling auto-acetylation of hMOF to affect gene regulation and DNA repair function. *Nucleic Acids Res* 2017;**45**:672–84.
22. Zhang R, Erler J, Langowski J. Histone acetylation regulates chromatin accessibility: role of H4K16 in inter-nucleosome interaction. *Biophys J* 2017;**112**:450–59.
23. Tanaka T, Izawa K, Maniwa Y *et al.* ETV2-TET1/TET2 complexes induce endothelial cell-specific Robo4 expression via promoter demethylation. *Sci Rep* 2018;**8**:5653.

24. Ramirez RD, Sheridan S, Girard L *et al*. Immortalization of human bronchial epithelial cells in the absence of viral oncoproteins. *Cancer Res* 2004;**64**:9027–34.
25. Corces MR, Trevino AE, Hamilton EG *et al*. An improved ATAC-seq protocol reduces background and enables interrogation of frozen tissues. *Nat Methods* 2017;**14**:959–62.
26. Luo Y, Hitz BC, Gabdank I *et al*. New developments on the Encyclopedia of DNA Elements (ENCODE) data portal. *Nucleic Acids Res* 2020;**48**:D882–9.
27. Consortium EP. An integrated encyclopedia of DNA elements in the human genome. *Nature* 2012;**489**:57–74.
28. Langmead B, Salzberg SL. Fast gapped-read alignment with Bowtie 2. *Nat Methods* 2012;**9**:357–59.
29. Zhang Y, Liu T, Meyer CA *et al*. Model-based analysis of ChIP-Seq (MACS). *Genome Biol* 2008;**9**:R137.
30. Tu S, Li M, Chen H *et al*. MAnorm2 for quantitatively comparing groups of ChIP-seq samples. *Genome Res* 2021;**31**:131–45.
31. Heinz S, Benner C, Spann N *et al*. Simple combinations of lineage-determining transcription factors prime cis-regulatory elements required for macrophage and B cell identities. *Mol Cell* 2010;**38**:576–89.
32. Lambert SA, Yang AWH, Sasse A *et al*. Similarity regression predicts evolution of transcription factor sequence specificity. *Nat Genet* 2019;**51**:981–89.
33. Harley JB, Chen X, Pujato M *et al*. Transcription factors operate across disease loci, with EBNA2 implicated in autoimmunity. *Nat Genet* 2018;**50**:699–707.
34. Andrews S. FastQC: a quality control tool for high throughput sequence data. 2010.
35. Martin M. Cutadapt removes adapter sequences from high-throughput sequencing reads. *EMBnet* 2011;**17**:3.
36. Li B, Dewey CN. RSEM: accurate transcript quantification from RNA-seq data with or without a reference genome. *BMC Bioinf* 2011;**12**:323.
37. Love MI, Huber W, Anders S. Moderated estimation of fold change and dispersion for RNA-seq data with DESeq2. *Genome Biol* 2014;**15**:550.
38. Soneson C, Love M, Robinson M. Differential analyses for RNA-seq: transcript-level estimates improve gene-level inferences. version 1; peer review: 2 approved. *F1000Research* 2015;**4**:1521.
39. Kartashov AV, Barski A. BioWardrobe: an integrated platform for analysis of epigenomics and transcriptomics data. *Genome Biol* 2015;**16**:158.
40. Ross-Innes CS, Stark R, Teschendorff AE *et al*. Differential oestrogen receptor binding is associated with clinical outcome in breast cancer. *Nature* 2012;**481**:389–93.
41. Whyte Warren A, Orlando David A, Hnisz D *et al*. Master transcription factors and mediator establish super-enhancers at key cell identity genes. *Cell* 2013;**153**:307–19.
42. Lovén J, Hoke Heather A, Lin Charles Y *et al*. Selective inhibition of tumor oncogenes by disruption of super-enhancers. *Cell* 2013;**153**:320–34.
43. Quinlan AR, Hall IM. BEDTools: a flexible suite of utilities for comparing genomic features. *Bioinformatics* 2010;**26**:841–42.
44. Laufer BI, Hwang H, Jianu JM *et al*. Low-pass whole genome bisulfite sequencing of neonatal dried blood spots identifies a role for RUNX1 in Down syndrome DNA methylation profiles. *Hum Mol Genet* 2020;**29**:3465–76.
45. Krueger F, Andrews SR. Bismark: a flexible aligner and methylation caller for Bisulfite-Seq applications. *Bioinformatics (Oxford, England)* 2011;**27**:1571–72.
46. Ewels P, Magnusson M, Lundin S *et al*. MultiQC: summarize analysis results for multiple tools and samples in a single report. *Bioinformatics* 2016;**32**:3047–48.
47. Laufer BI, Hwang H, Vogel Ciernia A *et al*. Whole genome bisulfite sequencing of Down syndrome brain reveals regional DNA hypermethylation and novel disorder insights. *Epigenetics* 2019;**14**:672–84.
48. Korthauer K, Chakraborty S, Benjamini Y *et al*. Detection and accurate false discovery rate control of differentially methylated regions from whole genome bisulfite sequencing. *Biostatistics* 2018;**20**:367–83.
49. Hansen KD, Langmead B, Irizarry RA. BSmooth: from whole genome bisulfite sequencing reads to differentially methylated regions. *Genome Biol* 2012;**13**:R83.
50. Subramanian A, Tamayo P, Mootha VK *et al*. Gene set enrichment analysis: a knowledge-based approach for interpreting genome-wide expression profiles. *Proc Natl Acad Sci* 2005;**102**:15545–50.
51. McErlean P, Kelly A, Dhariwal J *et al*. Profiling of H3K27Ac reveals the influence of asthma on the epigenome of the airway epithelium. *Front Genet* 2020;**11**:585746.
52. Cardenas A, Sordillo JE, Rifas-Shiman SL *et al*. The nasal methylome as a biomarker of asthma and airway inflammation in children. *Nat Commun* 2019;**10**:3095.
53. Forno E, Wang T, Qi C *et al*. DNA methylation in nasal epithelium, atopy, and atopic asthma in children: a genome-wide study. *Lancet Respir Med* 2019;**7**:336–46.
54. Zhu T, Zhang X, Chen X *et al*. Nasal DNA methylation differentiates severe from non-severe asthma in African-American children. *Allergy* 2021;**76**:1836–45.
55. Morin A, Thompson EE, Helling BA *et al*. A functional genomics pipeline to identify high-value asthma and allergy CpGs in the human methylome. *J Allergy Clin Immunol* 2023;**151**:1609–21.
56. Li D, Hsu S, Purushotham D *et al*. WashU Epigenome Browser update 2019. *Nucleic Acids Res* 2019;**47**:W158–65.
57. Lio CJ, Rao A. TET enzymes and 5hmC in adaptive and innate immune systems. *Front Immunol* 2019;**10**:210.
58. Wang H, Maurano MT, Qu H *et al*. Widespread plasticity in CTCF occupancy linked to DNA methylation. *Genome Res* 2012;**22**:1680–88.
59. Maurano MT, Wang H, John S *et al*. Role of DNA methylation in modulating transcription factor occupancy. *Cell Rep* 2015;**12**:1184–95.
60. Zhong Z, Feng S, Duttke SH *et al*. DNA methylation-linked chromatin accessibility affects genomic architecture in *Arabidopsis*. *Proc Natl Acad Sci USA* 2021;**118**:e2023347118.
61. Booth MJ, Ost TW, Beraldi D *et al*. Oxidative bisulfite sequencing of 5-methylcytosine and 5-hydroxymethylcytosine. *Nat Protoc* 2013;**8**:1841–51.
62. Calderon MA, Linneberg A, Kleine-Tebbe J *et al*. Respiratory allergy caused by house dust mites: what do we really know? *J Allergy Clin Immunol* 2015;**136**:38–48.
63. Platts-Mills TA, Erwin EA, Heymann PW *et al*. Pro: the evidence for a causal role of dust mites in asthma. *Am J Respir Crit Care Med* 2009;**180**:109–13; discussion 20-1.
64. Heintzman ND, Hon GC, Hawkins RD *et al*. Histone modifications at human enhancers reflect global cell-type-specific gene expression. *Nature* 2009;**459**:108–12.
65. Jung JU, Ravi S, Lee DW *et al*. NIK/MAP3K14 regulates mitochondrial dynamics and trafficking to promote cell invasion. *Curr Biol* 2016;**26**:3288–302.
66. Hnisz D, Abraham BJ, Lee TI *et al*. Super-enhancers in the control of cell identity and disease. *Cell* 2013;**155**:934–47.

67. Zhu T, Brown AP, Cai LP *et al*. Single-cell RNA-seq analysis reveals lung epithelial cell type-specific responses to HDM and regulation by Tet1. *Genes* 2022;**13**:880.
68. Kramer F, Torzewski J, Kamenz J *et al*. Interleukin-1beta stimulates acute phase response and C-reactive protein synthesis by inducing an NFkappaB- and C/EBPbeta-dependent autocrine interleukin-6 loop. *Mol Immunol* 2008;**45**:2678–89.
69. Emmanuel TO, Corry-Anke B, Wim T *et al*. Current perspectives on the role of interleukin-1 signalling in the pathogenesis of asthma and COPD. *Eur Respir J* 2020;**55**:1900563.
70. Wu X, Zhang Y. TET-mediated active DNA demethylation: mechanism, function and beyond. *Nat Rev Genet* 2017;**18**:517–34.
71. Zhang Q, Zhao K, Shen Q *et al*. Tet2 is required to resolve inflammation by recruiting Hdac2 to specifically repress IL-6. *Nature* 2015;**525**:389–93.
72. Chrysanthou S, Tang Q, Lee J *et al*. The DNA dioxygenase Tet1 regulates H3K27 modification and embryonic stem cell biology independent of its catalytic activity. *Nucleic Acids Res* 2022;**50**:3169–89.
73. Ito K, Lee J, Chrysanthou S *et al*. Non-catalytic roles of Tet2 are essential to regulate hematopoietic stem and progenitor cell homeostasis. *Cell Rep* 2019;**28**:2480–90e4.
74. Chen Q, Chen Y, Bian C *et al*. TET2 promotes histone O-GlcNAcylation during gene transcription. *Nature* 2013;**493**:561–64.
75. Sayeed SK, Zhao J, Sathyanarayana BK *et al*. C/EBPbeta (CEBPB) protein binding to the C/EBP|CRE DNA 8-mer TTGC|GTCA is inhibited by 5hmC and enhanced by 5mC, 5fC, and 5caC in the CG dinucleotide. *Biochim Biophys Acta* 2015;**1849**:583–89.
76. Huang G, Liu L, Wang H *et al*. Tet1 deficiency leads to premature reproductive aging by reducing spermatogonia stem cells and germ cell differentiation. *iScience* 2020;**23**:100908.
77. Wu BK, Brenner C. Suppression of TET1-dependent DNA demethylation is essential for KRAS-mediated transformation. *Cell Rep* 2014;**9**:1827–40.
78. Neri F, Incarnato D, Krepelova A *et al*. Genome-wide analysis identifies a functional association of Tet1 and Polycomb repressive complex 2 in mouse embryonic stem cells. *Genome Biol* 2013;**14**:R91.
79. Li Y, Zheng H, Wang Q *et al*. Genome-wide analyses reveal a role of Polycomb in promoting hypomethylation of DNA methylation valleys. *Genome Biol* 2018;**19**:18.
80. Dixon G, Pan H, Yang D *et al*. QSER1 protects DNA methylation valleys from de novo methylation. *Science* 2021;**372**.
81. van der Veer BK, Chen L, Custers C *et al*. Dual functions of TET1 in germ layer lineage bifurcation distinguished by genomic context and dependence on 5-methylcytosine oxidation. *Nucleic Acids Res* 2023;**51**:5469–98.
82. Zhu F, Zhu Q, Ye D *et al*. Sin3a-Tet1 interaction activates gene transcription and is required for embryonic stem cell pluripotency. *Nucleic Acids Res* 2018;**46**:6026–40.
83. Stolz P, Mantero AS, Tvardovskiy A *et al*. TET1 regulates gene expression and repression of endogenous retroviruses independent of DNA demethylation. *Nucleic Acids Res* 2022;**50**:8491–511.
84. Barter MJ, Cheung K, Falk J *et al*. Dynamic chromatin accessibility landscape changes following interleukin-1 stimulation. *Epigenetics* 2021;**16**:106–19.
85. Drake LY, Kita H. IL-33: biological properties, functions, and roles in airway disease. *Immunol Rev* 2017;**278**:173–84.
86. Poulain-Godefroy O, Boute M, Carrard J *et al*. The aryl hydrocarbon receptor in asthma: friend or foe? *Int J Mol Sci* 2020;**21**:8797.
87. Pugacheva EM, Kubo N, Loukinov D *et al*. CTCF mediates chromatin looping via N-terminal domain-dependent cohesin retention. *Proc Natl Acad Sci USA* 2020;**117**:2020–31.
88. Khoury A, Achinger-Kawecka J, Bert SA *et al*. Constitutively bound CTCF sites maintain 3D chromatin architecture and long-range epigenetically regulated domains. *Nat Commun* 2020;**11**:54.
89. Holwerda SJ, de Laat W. CTCF: the protein, the binding partners, the binding sites and their chromatin loops. *Philos Trans R Soc Lond B Biol Sci* 2013;**368**:20120369.
90. Holwerda S, de Laat W. Chromatin loops, gene positioning, and gene expression. *Front Genet* 2012;**3**:217.
91. Schmiedel BJ, Seumois G, Samaniego-Castruita D *et al*. 17q21 asthma-risk variants switch CTCF binding and regulate IL-2 production by T cells. *Nat Commun* 2016;**7**:13426.
92. Helling BA, Sobreira DR, Hansen GT *et al*. Altered transcriptional and chromatin responses to rhinovirus in bronchial epithelial cells from adults with asthma. *Commun Biol* 2020;**3**:678.

Environmental Epigenetics, 2025, 11(1), dvaf007 , DOI: https://doi.org/10.1093/eep/dvaf007, Advance Access Publication 20 March 2025, Research Article
Received 27 September 2024; Revised 18 February 2025; Accepted 19 March 2025